Lawrence Berkeley National Laboratory
LBL Publications

Title
Coupling fracture facies with in-situ permeability measurements to generate stochastic simulations of tight carbonate aquifer properties: Example from the Lower Cretaceous aquifer, Northern Provence, SE France

Permalink

Journal

ISSN

Authors
Bruna, Pierre-Olivier
Guglielmi, Yves
Viseur, Sophie
et al.

Publication Date

DOI

Peer reviewed

Coupling fracture facies with in-situ permeability measurements to generate stochastic simulations of tight carbonate aquifer properties: Example from the Lower Cretaceous aquifer, Northern Provence, SE France

Author links open overlay panel Pierre-OlivierBruna[a] YvesGuglielmi[a] SophieViseur[a] JulietteLamarche[a] OlivierBildstein[b]
Show more

Highlights

- Definition of fracture and permeability facies from hydrogeological data.

- Distribution permeable geobodies are more influenced by faults than by fractures.

- The diffuse fracturing plays a key role on fluid flow.

Summary

The relationships between fracture facies and permeability distribution have been explored using a well-constrained 3D implicit structural model of hemipelagic low porosity/low permeability carbonate from the Northern Provence region, SE France. Fracture and permeability facies were determined using an extensive dataset of 99 hydrogeological wells.

Data processing was undertaken using a step-by-step approach, involving: (i) identification of the fracture facies based on well logs detailing structure and stratigraphy; (ii) determination of permeability facies from the *a priori* correlation between the dimension of the hydraulic radius of influence (deduced from slug test analyses) and the type of reservoir heterogeneity (fissure, fracture, fault zone, etc.); (iii) three dimensional plot of fracture and permeability facies in the geological model using a variographic analysis of data.

Thirty-three sequential indicator simulations (SIS) based on geostatistic analyses were realised on both fracture and permeability facies. Finally, a connectivity algorithm was

developed to compute the probability of connection between selected infiltration areas and the major aquifer springs via moderate- to high-permeability geological bodies. Key results are: (i) fault zones have a greater role in controlling permeability facies distribution than on fracture facies repartition; (ii) there is little correlation between permeability and fracture facies distributions; (iii) connectivity results highlight the compartmentalisation of aquifers in the Cadarache area, the extensions of permeable geological bodies being limited by the N130 faults.

- **Previous** article in issue
- **Next** article in issue

Keywords

Geostatistics
Slug test
Fracture facies
Permeability facies
Tight reservoir
Carbonates

1. Introduction

Understanding fluid flow in aquifers is of primary importance in the context of current water demand increases and in tracking the subsurface spread of materials introduced into the subsurface, including pollutants. Accurate flow predictions require key geological heterogeneities that affect the aquifer at different scales to be correctly identified and represented in flow models. To a first approximation, aquifers are defined by the distribution of host rock (or matrix) petrophysical properties (porosity and permeability) that can be represented in flow models by flow units that correlate with rock type and depositional facies. Such porous aquifers differ from fractured or karstified aquifers (Gilli et al., 2008) where fracture and cave conduits may or may not be localised in specific rock types. The reality of aquifers containing fractures and caves can be complex. Workers have used double (Carniero, 2009) or even triple porosity models (Motyka et al., 1998, Wu et al., 2004) where flow heterogeneity reflects variability in both the matrix and some combination multi-scale structural objects. Often these models do not completely take into account the subsurface reality, which can be partly due to the presence and the effectiveness (or not) of structural features (Berkowitz, 2002). For example Rzonca (2008) studied a highly productive carbonate aquifer in Holy Cross Mountain, Poland. He demonstrated that the matrix in

this example is inactive and pointed out the singularity of this situation – as usually the matrix act as storage capacity in carbonate rock massifs. In the oil and gas industry, unconventional and fractured reservoirs with low matrix porosity and permeability can release huge amount of fluids (Zou, 2013). This example highlights the importance of both very small pores ranging down to the nanometre scale (Nelson, 2009, Loucks et al., 2012) and fracture populations that can be very complex (Laubach et al., 2009). Small faults and populations of opening-mode fractures can vary markedly in length, height (and heights pattern), aperture, the degree and pattern of mineral fill, as well as in density and spacing patterns and these relations can vary systematically with the stratigraphy (for example, Hooker et al., 2013). Such fracture population complexity can affect fluid flow. Guerriero et al. (2013) in their study of carbonate rocks from the Sorrento Peninsula (Italy) show a hierarchical organisation of permeable structures in a reservoir analogue and discriminate the relative role of these structures in fluid flow. Therefore, it remains challenging to represent these highly heterogeneous media at depth when only sparse data are available. The question of how to represent the dimensions of these heterogeneities in aquifers can benefit from the use of tools developed in the petroleum industry. For example, 3D modelling and geostatistics that can provide an interesting alternative to simpler conceptual models. The generation of multiple equiprobable models in a well-constrained structural framework will lead to a better representation of the subsurface heterogeneities. The applicability of these methods to groundwater modelling was broadly investigated in several papers (Biteman et al., 2004, Renard, 2007). Here to better account for structural and petrophysical heterogeneities we use a three-dimensional model to represent the reservoir architecture, including stratigraphic surfaces and faults, to describe the Lower Cretaceous limestone aquifer in Northern Provence. A pixel-based stochastic method, such as the one used in sedimentary facies simulation, is seldom considered to model faults and fractures in reservoirs (Renard, 2007, Pöppelreiter et al., 2008). These methods require generating a large number of equiprobable models to be reliable, which is time consuming and requires high performance software. In this paper, we address the question of how stochastic reservoir simulation can be used to predict dimension, location and degree of connectivity of fractured geobodies in a tight carbonate aquifer by defining an approach that allows restricting the numerical flow calculations to a reduced number of significantly different cases of static reservoir heterogeneities.

2. The Durance hemipelagic carbonates hydrogeological context

The area of interest is located 80 km North of Marseille, in the Durance Valley (SE France, Fig. 1). Its paleogeographic location is in the southern limb of the Vocontian Basin, where Berriasian to Valanginian sediments are interpreted to have been deposited in a slope-to-basin transition zone (Stampfli and Borel, 2002, Gréselle and Pittet, 2010). Previous work of Bruna et al. (2013) defined 2 groups of formations: mud-dominated (Upper Berriasian – Mid-Lower Valanginian age) 150 m thick, and grain-dominated (Mid-Lower Valanginian – end of Lower Valanginian age) 130–150 m thick (Fig. 1). Mud-dominated formations were deposited in low hydrodynamism environments, and are characterised by a low 0–4% porosity micritic matrix. This group is composed of 2 sedimentary formations:
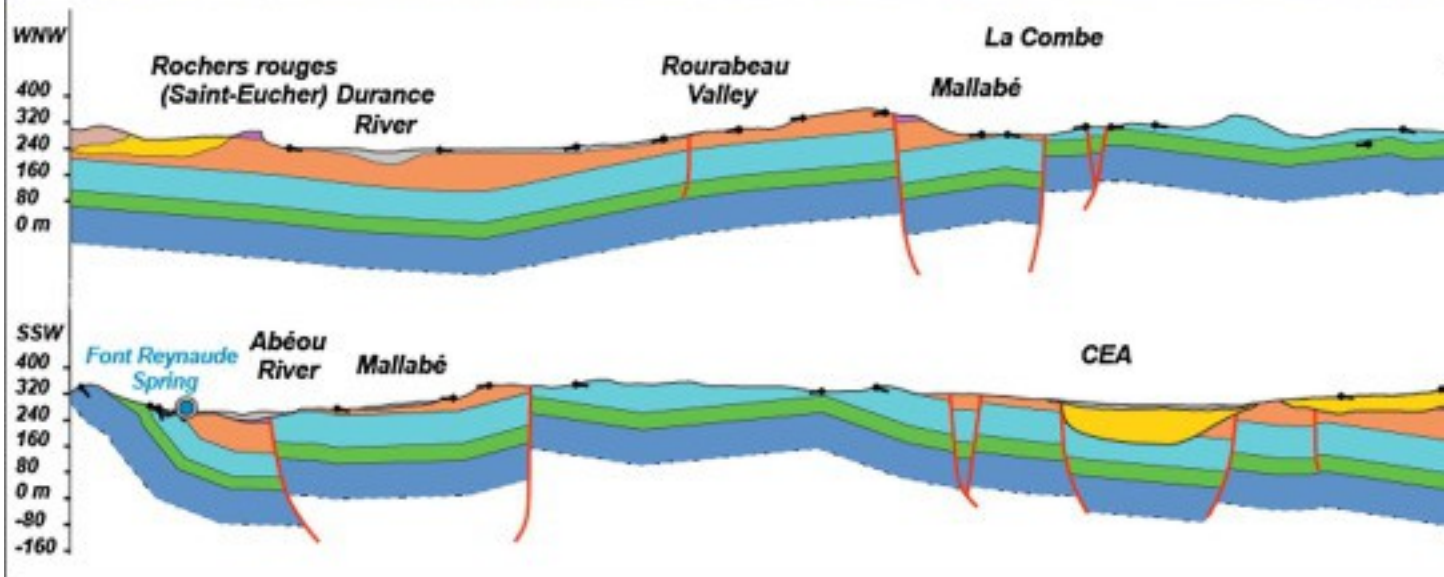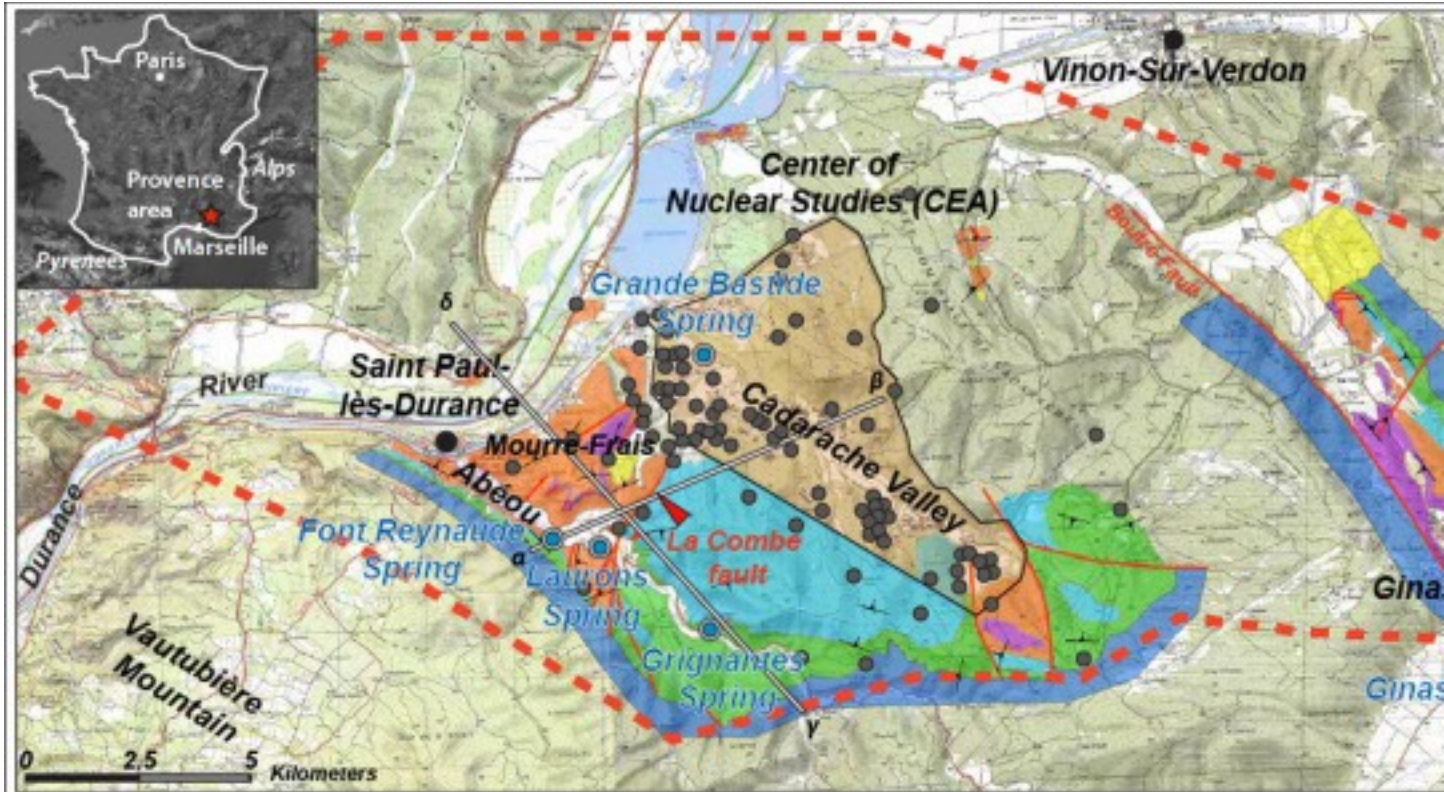
–

> Meyrargues Limestones Formation (1) is composed of metric to plurimetric grey to yellow planar beds, alternating with centimetre to pluri-centimetre thick laminated purple coloured beds.
>
> –
>
> Beaumont-de-Pertuis Limestones Formation (2) displays metric light brown nodulous beds alternating with metre to plurimeter thick yellow platy-limestone beds.

Fig. 1. Geological map of the Durance region including the dimensions of the 3D geological model and the location of boreholes. Synthetic lithostratigraphic column of the Tithonian to Valanginian interval ages on the right side of the log are based on ammonites and calpionellids biostratigraphic charts. Orthogonal cross sections thought

the area of interest emphasise the structural style and the thickness variations of the sedimentary units.

Grain-dominated formations correspond to higher energy environments and are typically characterised by significantly larger porosities up to 9%. This group is composed of 2 sedimentary formations:

–

> Saint Paul-lès-Durance Limestone Formation (3) is composed of pluri-centimetre to metre thick beds that form pluri-decameter lens-shaped bodies.

> –

> Saint Eucher Limestones Formation (4) is composed of grey limestone characterised by up to one metre thick stacked sand waves.

The present-day structure of South-East France records a complex and polyphase tectonic history. Deformation of the sedimentary succession produced E–W oriented anticlines separated by quiet zones (Lamarche et al., 2012) and major N030 transfer faults which were reactivated during polyphase deformation (Middle Durance Fault). The studied aquifer is located in a low deformation zone of the northern flank of the Vautubière Mountain (E–W – Southward verging anticline). This zone is affected by series of N120–N140 and N040–N060 faults. N120–N140 faults lengths (map traces) vary from 1.8 km to more than 6.5 km, and fault zone spacing is 1–2 km. These faults display strike-slip movement with normal apparent offsets (Guyonnet-Benaize et al., 2011, Masse and Masse, 2009). In the *CEA Cadarache* area, faults bound a dissymmetric graben filled with Tertiary and Quaternary deposits. N040–N060 faults are divided in two classes: major faults displaying lengths exceeding 1000 m and a 1064 m spacing and minor faults displaying lengths smaller than 150 m and a 260 m spacing. All of the N040–N060 faults display strike-slip movements with a slight vertical component associated with low vertical offsets. The fracturation was studied on two quarry outcrops located in the Abéou Valley (Fig. 1). Two families of plurimetric open fractures respectively N040–N050 and N140 were measured. The fractures spacing varies from 10 centimetres to more than three metres.

Upper Berriasian to Lower Valanginian carbonates host a regional aquifer drained by four perennial springs with a maximum high-water outflow of 300 l s^{-1}. Three springs outflow in the Abéou River, which is a tributary of the Durance River. Drilling of more than 300 piezometric wells, by the *CEA Cadarache* (set on the aquifer watershed; Fig. 1), identified three reservoir units: ≈12 m thick shallow Quaternary alluvium, 20–250 m

thick Tertiary clastic deposits, and 1200 m thick Cretaceous–Jurassic limestone. In the Cadarache Valley, sectors of interest correspond to Quaternary and Tertiary deposits. According to Cartalade (2002) and to Guyonnet-Benaize et al. (2011), the Tertiary and the Quaternary aquifers are considered highly permeable reservoirs (10^{-7} to >10^{-4} m s^{-1}). Possible connections between the Tertiary aquifer and the deep Cretaceous–Jurassic aquifer may occur in the study area. Hydrogeological boundaries defined by the Boutre Fault, Mirabeau-Vautubière Anticline (Fig. 1), Triassic argillaceous and evaporitic layers, and the Callovian–Oxfordian marls are all considered impermeable boundaries. The Lower Cretaceous aquifer, the main focus of this study, is interpreted to be exclusively controlled by fractures. Large exposures of the Lower Cretaceous carbonate series which outcrop in the Abéou valley and ninety-nine wells that give access to the aquifer geology and hydraulic properties at depth were used in this work (Fig. 1).

3. Method: three-dimensional coupling of geological and hydrological data

3.1. Building the three-dimensional structural model

The implicit modelling method (Calcagno et al., 2008) was used to build the 3D structural model. Implicit surfaces (faults or stratigraphic units) are isovalues of a 3D scalar function field (Caumon et al., 2009, Cherpeau et al., 2010). The modelling is performed in a defined volume of interest (VOI), in which a UVT Transform® algorithm converts x, y, z coordinates into u, v, t coordinates, where (u, v) isovalue planes represent the stratigraphy and t a pseudo-time (chronology). Therefore, modelled horizons are then considered as paleo-geochronological surfaces. Several authors (Spottke et al., 2005, Bayer et al., 2011, Comunian et al., 2011) have pointed out the importance of representing complex geological structures for reliable groundwater flow studies. In this paper, the implicit modelling approach allows consistent modelling of complex 3D grids embedding "Y" faults and other complex tectonic structures by compiling different data sources in a unified framework. The SKUA® (Subsurface Knowledge Unified Approach) plug-in integrates the UVT technology and was used in the present study.

The 3D model dimension is 21 × 8 × 0.5 km. The resolution of the structural model was defined at 70 m in aerial and vertical directions. The 3D environment is limited by the top of the Callovian-Oxfordian surface (500–700 m depth), considered as the lower boundary of the model according to Guyonnet-Benaize et al. (2011), and by the highest topographic point (Z max. = 555 m, northern flank of the Vautubière Mountain) considered as the top of the model. This model is limited to the south by the Vautubière Mountain and northward by the Verdon River (Fig. 1). It is limited eastward by the

Ginasservis Graben and westward by the Mirabeau Anticline (Fig. 1). The model is centred on the Cadarache Valley and includes the Abéou Valley and the southern zone of Verdon River (Cadarache Federal Forest). The dataset contains 1D, 2D and 3D data. The 1D data are lithostratigraphic sections and outcrop observations from the Abéou Valley and from the Boutre Fault zone (Fig. 1). Seven lithostratigraphic sections (ranging from 10 to 130 m thick) have been logged in detail (1:100) in the Abéou Valley sector. Due to the shallow dip of Lower Cretaceous sedimentary strata, the complete stratigraphic succession has never been sampled. Nevertheless, all contacts between two successive units were observed and a synthetic log was proposed (Fig. 1). Marker horizons in wells from Cadarache Valley supplement these data. The well data contains information of Tertiary/Quaternary to Secondary rock contacts. Such contacts were used as marker horizons in order to constrain the base of the Tertiary/Quaternary erosive surface. All data have been referenced in the field using the Global Positioning System(WGS84) with a horizontal precision less than five metres. Location data were converted into the local coordinate system (Lambert III).

The 2D data comprise a *CEA Cadarache* map, two BRGM geological maps of Pertuis (Arlhac et al., 1970) and of Tavernes (Mennessier et al., 1966), and an accurate geological map at 1:5000 centred in Abéou Valley and in the Boutre fault (Fig. 1). Two hundred and fifty-four samples were collected from lithostratigraphic sections or randomly sampled in the field. Petrographic studies on each sample were undertaken in order to describe and map sedimentary facies types and to define petrophysical properties (Bruna et al., 2013). A series of 2 regional and 3 local balanced cross-sections were integrated to the 3D structural model. The 3D data comprises a compilation of point-sets and surfaces extracted from existing models (Guyonnet-Benaize et al., 2011) and corrected with new data detailed above.

A grid was then generated to be consistent with field observations conducted on the outcrops. Consequently the dimensions of each grid cell are 11 × 11 × 10 m.

3.2. Geostatistical analyses

Stochastic simulations aim at generating several models of property or facies, conditioned to available data, for statistical analyses and risk assessment. In this paper, simulations were performed following the SIS algorithm (Sequential Indicator Simulation) (Goovaerts, 1997). The SIS method considers discrete variables. These variables are first kriged, and then the algorithm chooses an occurrence probability for the considered variable on each cell of the gridded model. Advantages of this method are: fast realisation, high potential for matching hard conditioning data, and capacity to

reproduce different facies geometries in a model. The SIS presented in this paper is conditioned to well data only (hard conditioning data), variograms and global proportions.

3.2.1. Fracture facies

An extensive database of 99 wells drilled between 1984 and 2010 (part of a hydrogeological survey network) was provided by the *Cea Cadarache*. These wells are partially screened and intervals are mainly shallow (mean depth is 75.4 m with a standard deviation of 57 m). Check-in quality (camera) and re-habilitation of wells were done every year since 2009. Each well has an associated drilling log, its resolution and precision dependent on the operator, the drilling type (destructive or cored) and the location of the well. Several well reports contain additional information such as physical parametres of the drilling machine (velocity of the drilling tool = VIA), detailed well logs, identification of major structures (karst and faults), camera investigation, core investigations, geotechnical tests (Lefranc, Lugeon tests) and estimation of the permeability (Cassan's method) Cassan (1978).

A first step analysis of well logs and reports allowed identifying three main fracture facies:

- Facies FF1 is a non-fractured facies. FF1 has been assigned when well logs describe the host rock (fracture devoided or containing negligible amount of sealed fracture).

- Facies FF2 is a fractured facies composed of various fracture types and sizes, including faults.

- Facies FF3 is a karstified facies, represented by empty or filled-with-clay cavities.
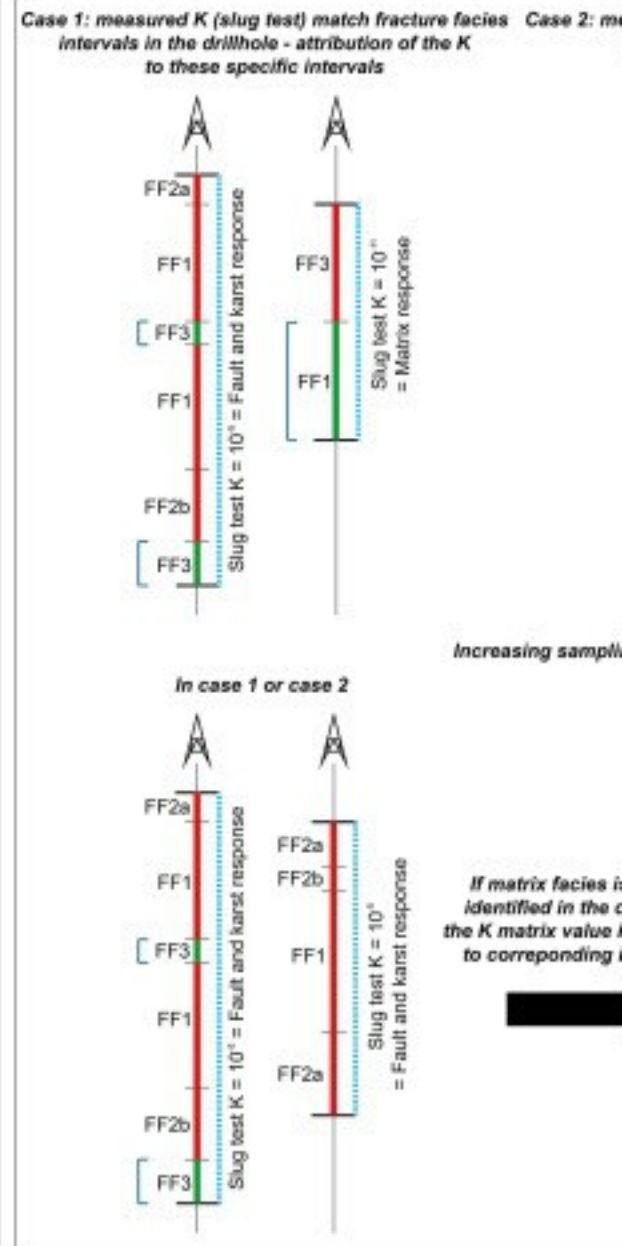
The main challenge of this first step analysis was to synthesise and to attribute a degree of confidence to well logs and descriptions. In order to evaluate this parameter, the study focused on both the interval length where facies is defined and the available additional information (Fig. 2). A score of 0–1 was attributed to each facies interval and is summarised in Table 1. For example, if the description of FF1 in a few metre long intervals is consistent with a camera investigation and/or drilling velocity, it is given a

better mark than the same facies defined on a hundred metre long interval without any additional information.

1. [Download high-res image (733KB)](#)
2. [Download full-size image](#)

Fig. 2. Methodology used to define the permeability intervals in the well screened interval. Sketches highlight the solution found to increase the sampling rate by taking into account well-defined non-fractured intervals.

Table 1. Definition of the occurrence probability of fracture [facies](#). The same method was applied to permeabilities facies investigation.

Probability	Observation interval							Additional Tool		
	Localised/systematic	<5 m	<10 m	<20 m	>20 m	Core observe	Detailed report	VIA-Geophysical tool	Camera	Overlap K
1 Non fractured limestones (FF1)										
0.1					O (present)					
0.2				O						
0.3			O							
0.4		O			O		O/N (optional)	O/N		
0.5				O			O/N	O/N		
0.6			O	O/N			O/N	O/N		
0.7		O	O/N				O/N	O/N		
0.8		O	O/N				O	O		
0.9		O	O/N				O	O		O
1.0		O	O/N			O/N	O	O		O/N	O/N
3 fractured/faulted limestones (FF2)										
0.1										
0.2										
0.3										
0.4			O/N		O			O/N		
0.5		O/N		O				O/N		
0.6			O				O/N	O/N		
0.7		O					O/N	O/N		
0.8	O	O/N					O	O/N		
0.9	O	O/N				O/N	O	O/N	O/N	
1.0	O	O/N				O	O	O	O	O
3 karstified limestones (FF3)										
0.1										
0.2										

Probability	Observation interval							Additional Tool		
	Localised/systematic	<5 m	<10 m	<20 m	>20 m	Core observe	Detailed report	VIA-Geophysical tool	Camera	Overlap K
0.3										
0.4										
0.5										
0.6										
0.7		O						O/N		
0.8	O/N	O						O/N		
0.9	O	O/N					O	O/N		
1.0	O	O/N				O	O	O/N	O	O

When the mark is lower than 0.5, the facies description was not considered with confidence, and was identified as a null value (−99,999).

Some log descriptions are very accurate and allow the separation of fractures in regard to their dimension. Consequently, the FF2 facies was divided in two additional facies:

- Facies FF2a is a fissure facies that contains multi-centimetre long fractures with small aperture (generally > 0.5 cm and considered as matched by drilling operators).

- Facies FF2b is a fracture facies that contains multi-decimetre to metre-long fractures with large aperture (generally > 1 cm and considered as open fracture by drilling operators).

3.2.2. Wells permeability

The hydraulic property of wells used for fracture facies identification was investigated during two hydraulic slug test campaigns in 2010 and 2012. Slug tests were used to evaluate local hydraulic properties of the aquifer. The protocol was to quickly change the static level of an aquifer by injecting a known quantity of water (Chapuis, 1998) and to monitor the return to the static water table. This study used the Cooper–Papadopulos–Bredehoeft solution available on the Hytool® software (Renard, 2003), to re-interpret the variation of the water level versus time and to estimate the transmissivity and the storage of the aquifer. This solution assumes that the tested

aquifer is an ideal [porous media](#) with a radial transmissivity and consequently could be considered as an infinite medium. In addition, [Bredehoeft and Papadopulos (1980)](#) solution considers aquifers with very low storage capacity (tight rocks). This solution also gives an estimate of the storage coefficient of a given aquifer by taking into account the well equipment compressibility ([Mejìas et al., 2009](#)). The method used is consequently more accurate than a simple Cooper solution. Permeability values were deduced by dividing the transmissivity with the well screen thickness.

The fracture dataset defined in wells was formatted to compare the fracture facies with the well permeability. Permeability was averaged from slug test results on the whole screened interval of each well. Well screen thickness is highly variable (standard deviation of approximately 31 m) and induces significant bias on the permeability estimation. To reduce this bias, the following two-step protocol was used:

(1)

Work of [Yang and Gates (1997)](#) demonstrates that the slug test radius of influence can be correlated with particular [geological features](#). Consequently, classes of permeability ranging from 10^{-14} to $>10^{-5}$ m s^{-1} has been defined as following:

-
[CK1](#) corresponds to permeability values of 10^{-14} to 10^{-11} m s^{-1} representative of matrix effects ([Fig. 3](#)).

The equation shown in the figure:

$$IR = \sqrt{15(T \times tps)/S}$$

T = transmissivity, tps = return time to static level
S = storativity

Legend

K Matrix (10^{-14}–10^{-13} m.s^{-1})	○	Permeability value measured in each well of the area of interest
K Fissures (10^{-10}–10^{-9} m.s^{-1})		
K Fractures (10^{-8}–10^{-6} m.s^{-1})	- - -	Facies cut-off
K Faults-Karsts (>10^{-6} m.s^{-1})	·--·	Best fit curve
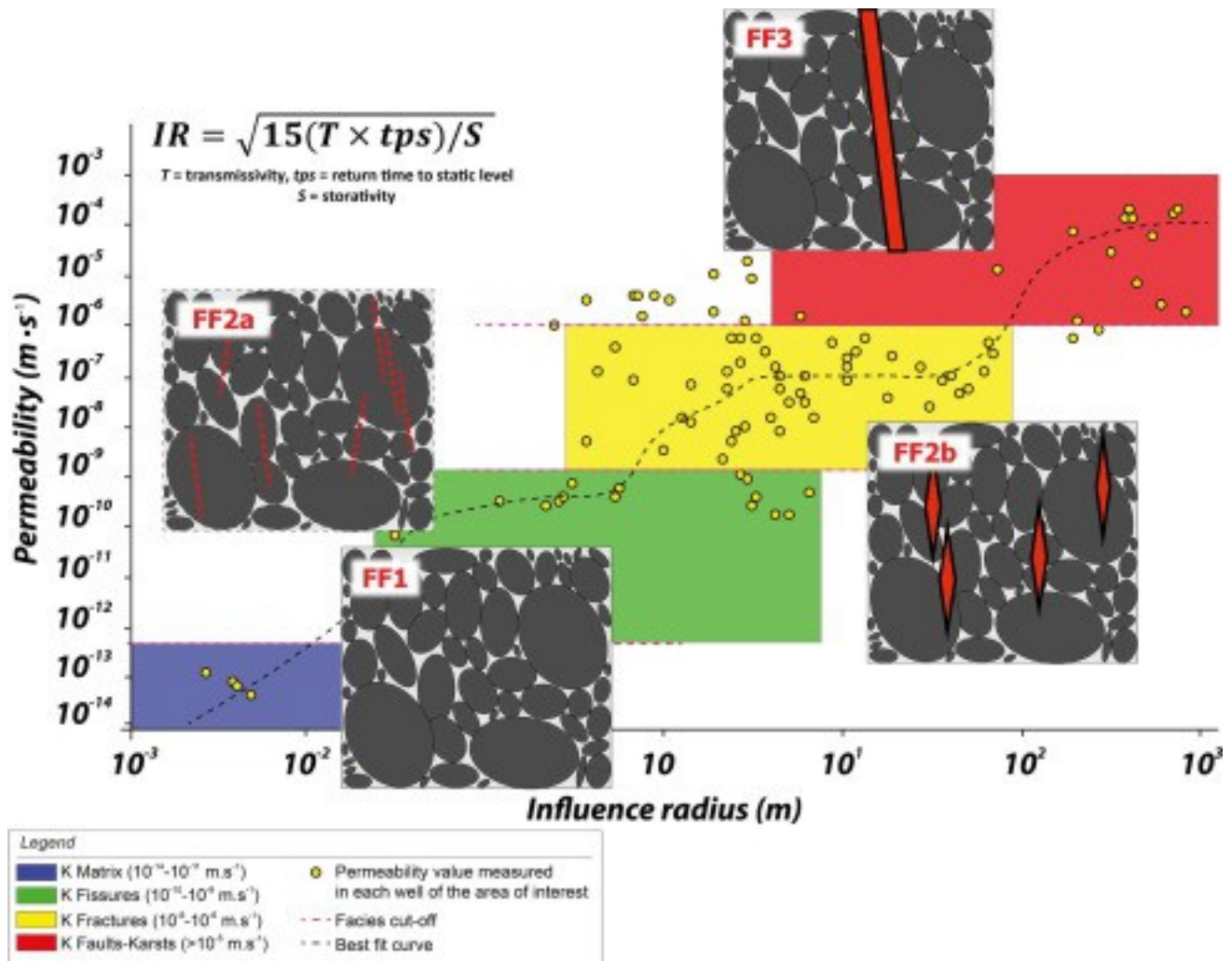
1. Download high-res image (399KB)
2. Download full-size image

Fig. 3. Link between fracture facies and slug tests influence radii. Yellow dots are measured permeability value in the studied wells. FF1 facies (matrix) is then characterised by a small influence radius close to the borehole (10^{-3} to 10^{-2} m) and with a low range of permeability (10^{-14} to 10^{-13} m s^{-1}). Facies cuts-offs were established in regards of the slug tests permeability curve inflexion. (For interpretation of the references to colour in this figure legend, the reader is referred to the web version of this article.)

-

CK2 corresponds to permeability values of 10^{-10} to 10^{-9} m s^{-1} representative of the fissure effects (Fig. 3).

-

CK3 corresponds to permeability of 10^{-8} to 10^{-6} m s^{-1} representative of fracture effects (Fig. 3).

- CK4 corresponds to permeability values above 10^{-5} m s^{-1} representative of fault and karst effects (Fig. 3).

(2)

These classes were compared with the fracture facies classification for each well. The method was to attribute the permeability value measured at the screen interval scale to a facies interval (Fig. 2). When the measured permeability did not match any facies described in the well, a null value was attributed to the entire well (Fig. 2).

The main caveat in this method was that the reduction of the intervals induced a significant decrease in the available point data for further simulations. This is mainly due to the quality of the well geological reports. For instance, if a well was described with open fractures on the entire screened interval and a permeability of 10^{-12} m s^{-1}, the well geological report was considered inconsistent. In order to increase the sampling rate, the matrix hydraulic properties were introduced into the dataset. When the matrix was identified with a high degree of certainty (occurrence probability over 0.6, see Section 3.2.1) this facies was assigned a 10^{-11} m s^{-1} permeability (lowest dataset value).

3.3. Comparison of simulations with field data

Thirty-three SIS simulations were generated for fracture and permeability facies. These simulation, analysed on one E–W cross-section and on a horizontal map of the top of the model were based on variogram analyses (Goovaerts, 1997, Armstrong, 1998, Gringarten and Deutsch, 2001). Different experimental variograms are computed and analysed in different directions to capture the facies anisotropy. Gringarten and Deutsch (2001)proposed an integrated protocol to analyse variograms. This approach was used in this paper to perform the variogram analyses. Variogram ranges represent an averaged estimate of facies dimensions (Guo and Deutsch, 2010). The spatial correlation is defined at short (range, correlation) but also at long distance (sill, simple variance). Analysing these parametres and the different variogram allows the geological structure geometries and organisation to be estimated.

A "connectivity algorithm" was developed to evaluate connectivity between selected areas in the fractured geobodies, identified in the stochastical modelling, and the major springs. This algorithm considers the degree of static connectivity, the dimensions and the rank of connected geobodies. Nevertheless, several other definitions exist (Deutsch, 1998, Knudby and Carrera, 2005) and a review of connectivity definitions is proposed in Renard and Allard (2013). In this study, the static connectivity corresponds to the

case where two cells with the same facies are connected if a continuous path (straight or tortuous) exists between these cells. In three dimensions, the connectivity is effective if only two surfaces of the cells are linked. The interface between Tertiary/Quaternary units and Cretaceous–Jurassic units was considered here as connected but recent work conducted on site tend to show that this hypothesis may not be verified everywhere.

4. Results

4.1. Three-dimensional structural model

The model contains 25 faults observed and measured in the field. Additional faults were observed but not considered here because of their poor surface expression or their relatively insignificant impact (offset) on the sedimentary succession. Vertical extent of these faults has been estimated based on the map trace length, related offset and dominant direction of movement. The model shows that N050 oriented faults measured in the Abéou Valley display only a very slight offset.

This solution reflects the consideration of the fault movement and the geological map realised in the area of interest. This is not the case for N130 faults that display large vertical offset of 100–400 m.

The 3D structural model displays a contrast between the north and the south of the Cadarache Valley. Tertiary or Quaternary units seal the faults. This results in a duality between the southern area of interest where faults are observed in outcrop (where the Cretaceous rocks are exposed) and the northern part where the faults affecting Mesozoicterranes are under-cover (where the Tertiary or Quaternary rocks crop out).
Eight stratigraphic horizons starting from the top of Callovian–Oxfordian layer to the topography are represented. The Secondary sedimentary succession is conformable and shows little thickness variation in the whole model. This is consistent with the present-day structural architecture of the Northern Provence, where fold and thrust belts are separated by wide, tabular, relatively undeformed zones (Lamarche et al., 2012).
The Lower Cretaceous layers are relatively thin (<350 m thick) compared to the whole Mesozoic succession (from 2000 to 2500 m thick from base Triassic to the top of the Lower Cretaceous). This implies that the Lower Cretaceous stratigraphy needs to be carefully modelled to provide an accurate framework for stochastic simulation process. SKUA® software allows modulation of the data point weight with the fitting factor. Using

a high fitting factor, modelled horizons match very well the point data rather than with a low fitting factor where horizons are smoothed. Thus, outcrop and cross section data points were implemented with a very-high fitting factor in order to tightly constrain horizons close to these points. This process sometimes produces artifacts at the data location that have been corrected manually by a local smoothing of the surfaces. [Fig. 4](), shows a thickness map of Formations (1)–(3) and the histogram of thickness value distribution.

–

> Formation (1) displays the lowest standard deviation on the thickness values (8 m). The median value (49 m) is consistent with the 50 m observed value in the Grignantes quarry ([Bruna et al., 2013]()).
>
> –
>
> Formation (2) shows the highest value of standard deviation (16 m). Nevertheless, the median value is here again consistent with outcrop measurements. The standard deviation value for Formation (2) is explained by extreme values repartition emphasising boundary and fault effects.
>
> –
>
> Formation (3) thickness median value (101 m) is slightly above the measured average value (80 m). This is consistent with previous interpretations of the [depositional environment]() ([Bruna et al., 2013]()) and field observations. Indeed, Formation 3 was interpreted as turbiditic–contouritic deposit by the previous authors ([Fig. 4]()).
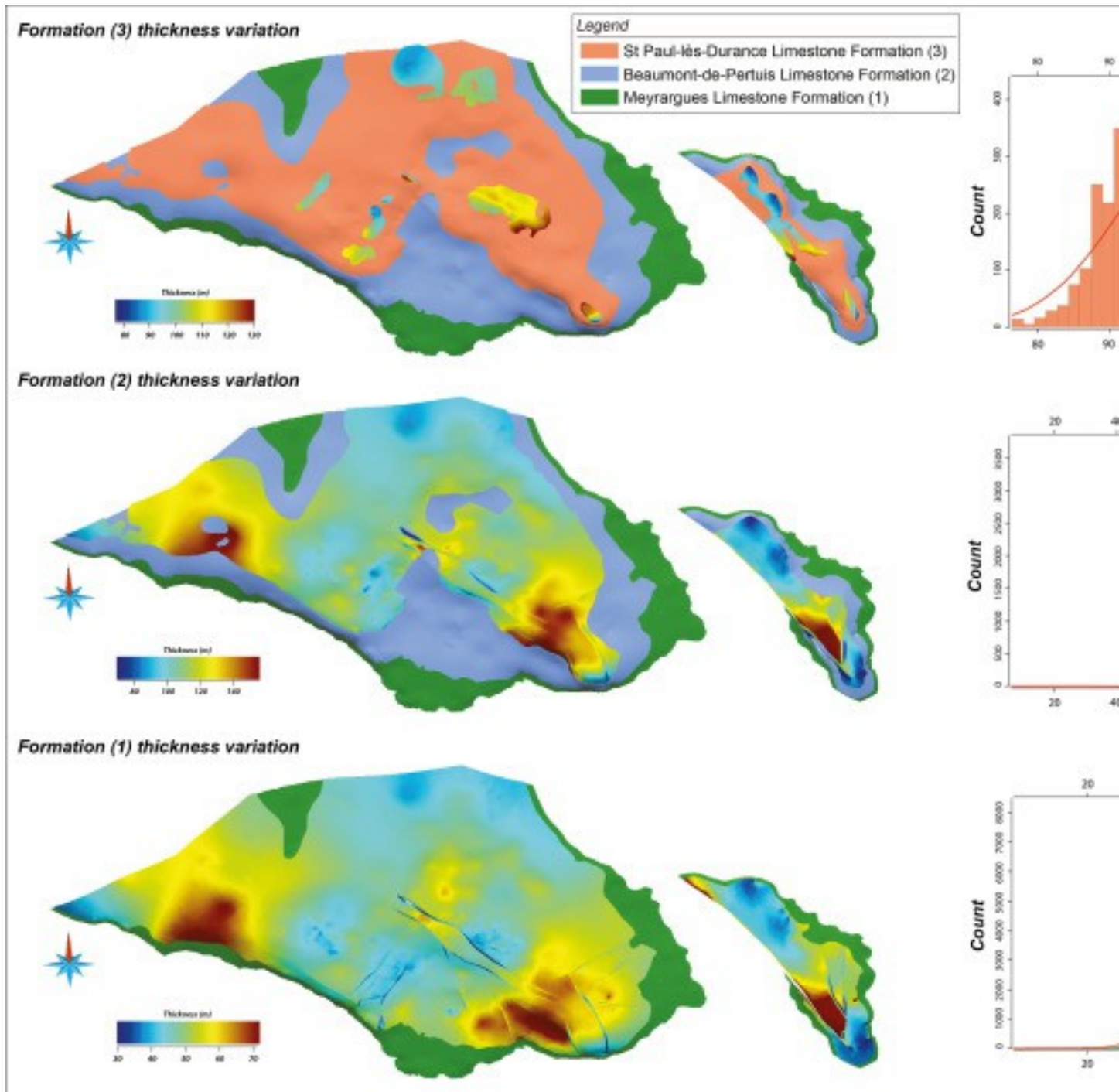
Fig. 4. Thickness maps of Formations (1)–(3). Main statistical data are indicated for each thickness maps.

These deviations are linked to the modelling process and mainly to the chosen resolution defined in the implicit modelling workflow. The provided thicknesses are in the

same order of magnitude than the measured sections in the field. This ensures the 3D structural framework consistent with the geological available information.

Appropriate cell dimensions were chosen in regard to stochastic simulations. Cells measure 11 × 11 × 10 m with a total volume of more than 89 million of cells. Because the Lower Cretaceous is the target of the present study, the Upper Jurassic successions were substracted from the grid. Stochastic simulations were not computed for Tertiary and Quaternary units (excluded as a region in the grid) but these volumes were afterwards used in the connectivity calculations as a one-cell volume connected with underlying units. The sampling of wells in the 3D grid was established in each cell centre along the well log. Fracture facies simulations have been performed with 2278 samples and permeability simulations with 878 samples.

4.2. Spatial anisotropy and variogram analyses

Global proportions calculated from well data are the following: non-fractured facies (FF1) is 42.8%, fractured facies (FF2) is 55.7% and karstified facies (FF3) is 1.5%; low permeability (CK1) is 52.1%, moderate permeability (CK2) is 21.9%, high permeability (CK3) is 20.4% and very high permeability (CK4) is 5.6%.

Following the SIS algorithm, fracture facies were investigated with three variables (FF1 to FF3). Permeability facies were provided with four variables (CK1 to CK4). Variograms were computed in the vertical and in several horizontal directions (N055, N068, N077, N090, N100, N110, N125, and N180; Table 2). Parametres of the ellipsoid issued from variogram modelling are: the first axis (Ra), the second axis (Rb) and the third axis (Rc).

Table 2. Synthesis of variograms behaviour. ZA is a Zonal Anisotropy, GA is a Geometric Anisotropy, HE is a Hole-Effect behaviour, T is a Trend behaviour, and E is an Erratic repartition of points in the experimental variogram. Small letters indicate that the observed behaviour is not clearly defined.
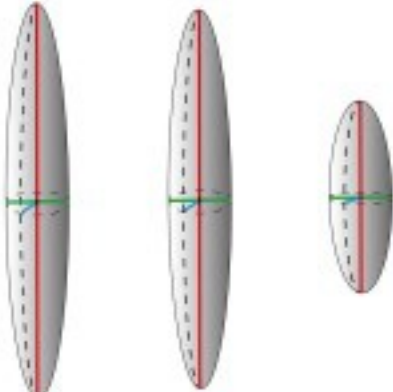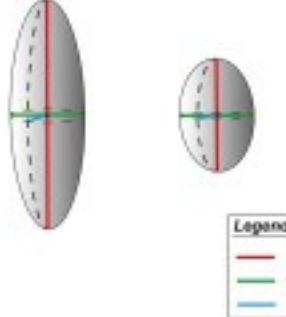
	Vertical variogram	Az N180 variogram	Az N125 variogram	Az N110 variogram	Az N100 variogram	Az N090 variogram	Az N077 variogram	Az N068 variogram	Az N055 variogram	
Facies FF1	ZA-E	HE	he	he	za	E	E	E	BF-E	
Facies FF2	ZA-E	HE	he	HE	E	E	t	E	BF-E	
Facies FF3	ZA	E	Za	E	E	E	E	AZ	bf-E	
Facies CK1	ZA	E	he	he	ZA	E	E	E	bf	

	Vertical variogram	Az N180 variogram	Az N125 variogram	Az N110 variogram	Az N100 variogram	Az N090 variogram	Az N077 variogram	Az N068 variogram	Az N055 variogram	
Facies CK2	ZA	E	HE	he	E	ZA	bf-ZA	ZA	ZA	
Facies CK3	ZA	E	E	ZA	ZA	E	E	E	BF-E	
Facies CK4	ZA	ZA	E	E	t	E	E	bf-E	E	

4.2.1. Fracture facies variograms

The spherical variogram model was chosen to fit experimental variograms (issued from dataset) of FF1–FF2–FF3 facies (Appendix A). Sills vary widely for each facies and express large scale variability (zonal anisotropy). Due to the grid resolution and the isolated occurrence of karstified facies (FF3), the main structure displays a binary arrangement: when the non-fractured facies is expressed, the fractured facies is absent and conversely.

FF1 and FF2 vertical variograms displays an erratic behaviour (Table 2) meaning that the sill is largely below the sampling variance. Such a behaviour implies a high vertical continuity of FF1 and FF2 facies.

Therefore, the range of the variogram model was extended to a very high lag distance in order to reproduce the continuity effect. The horizontal variogram is erratic within the N068, N077, N090, and the N100 directions implying a lack of representative pairs of data points in these directions. Yet, the variability could be more important in these directions rather than in the other ones. N110, N125 and N180 directions show a well-expressed hole-effect (Table 2) indicating a cyclicity in the facies occurring in these directions. The ellipsoids of FF1 and FF2 facies are oriented in the N055 direction (maximal correlation distance between pairs of points). Modelled geobodies emphasise an anisotropy where Ra = 2170, Rb = 369 and Rc = 340 for FF1 facies, and Ra = 2015 m, Rb = 369 m and Rc = 349 m for FF2 facies (Fig. 5). The FF3 vertical variogram displays a similar behaviour as previously observed in FF1 and FF2 but is smaller and rare in the model. Horizontal variograms highlight the low amount of available data points. Consequently, their behaviour is erratic in each computed directions (Table 2). Geobodies issued from variographic analyses emphasise a marked anisotropy where Ra = 612 m, Rb = 369 m and Rc = 242 m (Fig. 5).

		Facies FF1	Facies FF2	Facies FF3	Facies CK1	Facies CK2
	Global proportions	42.80%	55.70%	1.50%	52.10%	21.90%
	Variogram model	Spherical	Spherical	Spherical	Exponential	Exponential
	Sill	0.24	0.24	0.025	0.249	0.16
	Vertical range (dimensionless)	> 0.25	> 0.25	> 0.25	> 0.25	> 0.25
	Horizontal range 1 (dimensionless)	0.16	0.15	0.028	0.06	0.023
	Horizontal range 2 (dimensionless)	0.02	0.02	0.028	0.02	0.023
Ellipsoid parameters	A1	2168	2015	612	820	497
	A2	369	369	369	407	490
	A3	340	349	242	260	194
	Orientation	N055	N055	N055	N055	N055
Ellipsoide representation						

1. [Download high-res image (415KB)](#)
2. [Download full-size image](#)

Fig. 5. Variogram parametres synthesis including the model used to fit the experimental variograms, range and sill values, length of the ellipsoid axes and orientation of the great axis and representation of the relative size of facies ellipsoids.

4.2.2. Permeability variograms

The exponential model was chosen to fit experimental variograms of CK1–CK2–CK3–CK4 facies (Appendix B). Vertical variograms of these facies display a sill largely below the sampling variance. The same processing as the one applied for fracture facies was used in this case.

The CK1 horizontal variogram (Table 2) displays an erratic behaviour in N055, N068, N077, and N090. A slight hole-effect is identified in the N110 and N125 azimuths. The experimental variogram is slightly below the model in the N100 azimuth. This zonal anisotropy implies that the variability is not visible in such direction. The maximum range is reached for the N055 variogram. The variability of range within this facies implies a geometric anisotropy for CK1. The variographic behaviour is represented by an anisotropic ellipsoid with a $Ra = 820$ m, $Rb = 407$ m and $Rc = 260$ m (Fig. 5).
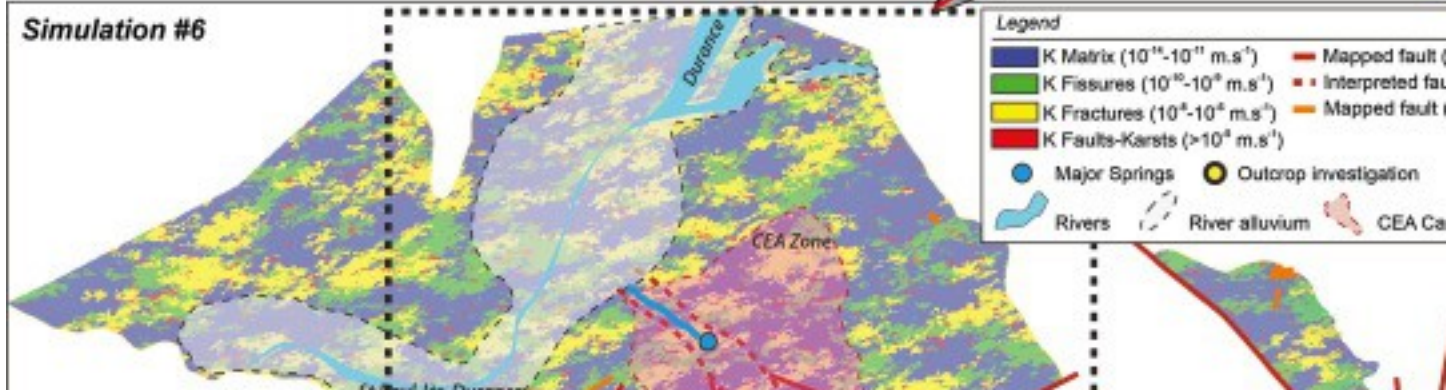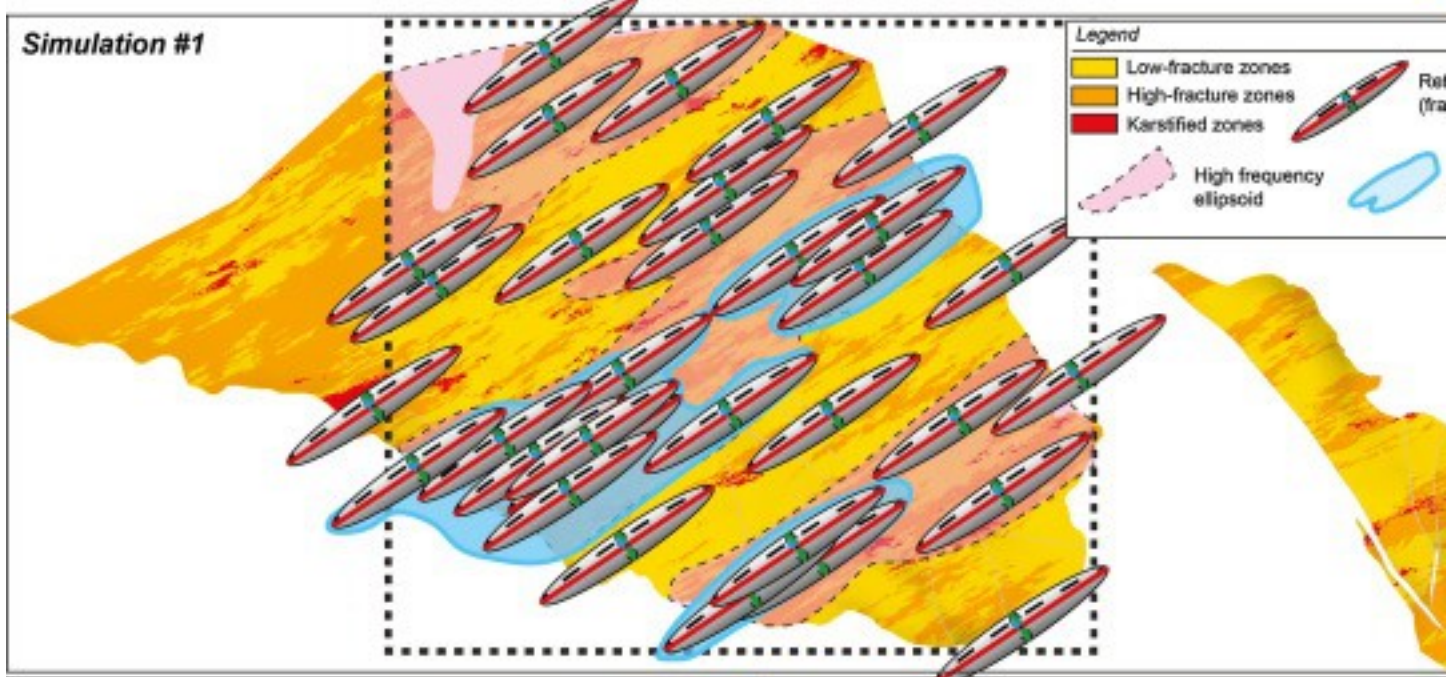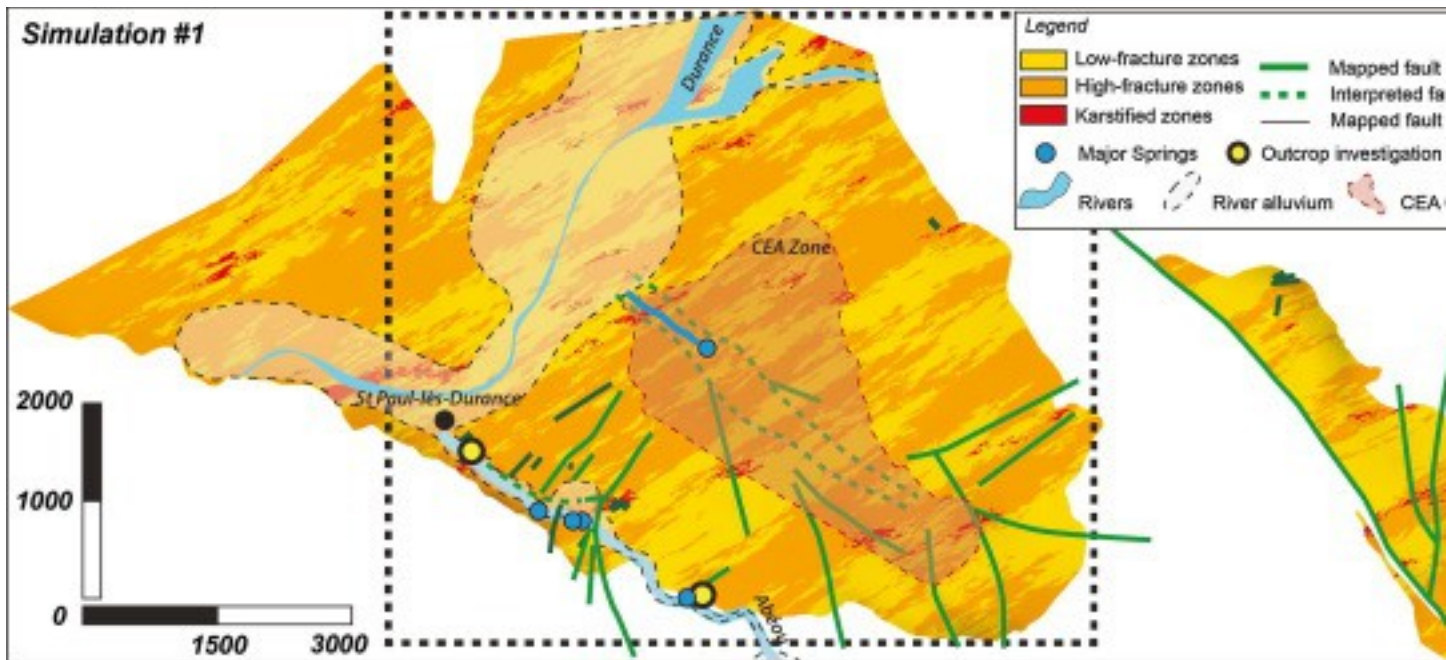
The CK2 vertical variogram is under the variance sill (zonal anisotropy) on N055, N068, N077, and N090 azimuths. N110 and N125 directions display hole-effects behaviours. CK2 horizontal variogram shows the same range in all directions (Fig. 5 and Table 2). The representative ellipsoid is more isotropic than in the CK1 facies with a Ra = 497 m, Rb = 490 m and Rc = 194 m (Fig. 5).

The CK3 horizontal variogram is erratic in the N068, N077, and N090 directions. N100 and N180 directions record a slight zonal anisotropy. The CK3 horizontal variogram (Table 2) displays a maximum range in the N055 direction. The ellipsoid representative of CK3 is clearly anisotropic with a Ra = 728 m, Rb = 498 m and Rc = 318 m (Fig. 5). CK4 horizontal variogram is erratic in almost all directions due to the punctual and the non-abundance of data points. The Direction N180 displays a zonal anisotropy and allows fitting the range. CK4 experimental variogram (Table 2) has a single range. The ellipsoid is again highly anisotropic with a Ra = 490 m, Rb = 97 m and Rc = 39 m (Fig. 5).

4.3. Organisation of fracture and permeability facies stochastic maps

Thirty-three fracture and permeability facies simulations have been performed to obtain a statistically representative population of 3D models. Fracture and permeability facies were investigated in details in an area that contained 50 of the 99 wells (Fig. 1). While simulation is a 3D process, a 2D view is shown, in order to observe the horizontal variability, the recurrence, and the dimensions of facies geobodies. In order to conduct such an analysis, the reference ellipsoid defined for each facies by the variographic analysis was compared to the facies maps resulting from the simulations (Fig. 6, summary in Table 3). In the case of fracture facies, the ellipsoid shape and orientation are the same between non-fractured facies (FF1 facies) and fractured facies (FF2 facies) (Fig. 6). Ellipsoids can be classified as three types: isolated ellipsoids; amalgamated ellipsoids representing large geobodies; and bands of amalgamated geobodies crossing the entire zone. The amalgamated geobodies correspond to FF1 and FF2 facies with a larger proportion of FF2 facies. These are large and discontinuous/tortuous geobodies oriented N055 with a limited and cyclic aerial extension (Fig. 6). These geobodies have a periodic spacing of 500–1500 m which is close to the periodicity of the faults observed in the field.

Simulation #1

Legend

- Low-fracture zones
- High-fracture zones
- Karstified zones
- Mapped fault
- Interpreted fa
- Mapped fault
- Major Springs
- Outcrop investigation
- Rivers
- River alluvium
- CEA

2000

1000

0

1500   3000

CEA Zone

Durance

St Paul-lès-Durance

Abo

Simulation #1

Legend

- Low-fracture zones
- High-fracture zones
- Karstified zones
- Re
- (fra
- High frequency ellipsoid

Simulation #6

Legend

- K Matrix (10^{-16}-10^{-11} m.s^{-1})
- K Fissures (10^{-10}-10^{-6} m.s^{-1})
- K Fractures (10^{-6}-10^{-5} m.s^{-1})
- K Faults-Karsts (>10^{-4} m.s^{-1})
- Mapped fault
- Interpreted fau
- Mapped fault
- Major Springs
- Outcrop investigation
- Rivers
- River alluvium
- CEA Ca

CEA Zone

Durance

Fig. 6. Geobodies size and organisation in the well-documented area limited by the maximal extension of [borehole](#) data. The reference [ellipsoid](#) of fractured [facies](#) was chosen to show geobodies repartition in the fracture facies simulation. Moderate and high permeability facies reference ellipsoid was chosen to evidence geobodies organisation in the permeability facies simulation.

Table 3. Synthesis of simulations matching field fault pattern. The table emphasises the type of geobody organisation deduced from each simulation for both fracture and permeability [facies](#).

	Facies Fracture simulation				Facies permeability simulation		
# of realisation	Fitting (Y–N)	Type of fitting	Aspect of non fitting (between Combe fault E–W parts)	# of realisation	Fitting (Y–N)	Type of fitting	Aspect of non fitting (between Combe fault E–W parts)
1	Y	Amalgamated		1	Y	Amalgamated-linear	
2	Y	Isolated		2	Y	Amalgamated	
3	N		Homogeneous	3	N		Inverse-linear
4	N		Homogeneous	4	Y	Amalgamated	
5	N		Homogeneous	5	N		Homogeneous
6	Y	Isolated		6	Y	Linear	
7	Y	Isolated		7	N		Homogeneous
8	Y	Amalgamated		8	Y	Amalgamated	
9	Y	Amalgamated		9	Y	Amalgamated	
10	N		Homogeneous	10	N		Homogeneous-linear
11	N		Inverse of expected	11	N		Homogeneous
12	Y	Isolated		12	Y	Amalgamated	
13	N		Inverse of expected	13	N		Homogeneous
14	N		Inverse of expected	14	N		Homogeneous
15	N		Homogeneous	15	Y	Amalgamated	
16	N		Homogeneous	16	Y	Amalgamated-linear	
17	Y	Amalgamated		17	Y	Amalgamated	
18	N		Homogeneous	18	N		Homogeneous-

Facies Fracture simulation				Facies permeability simulation			
# of realisation	Fitting (Y–N)	Type of fitting	Aspect of non fitting (between Combe fault E–W parts)	# of realisation	Fitting (Y–N)	Type of fitting	Aspect of non fitting (between Combe fault E–W parts)
							linear
19	N		Homogeneous	19	N		Homogeneous-linear
20	N		Homogeneous	20	N		Homogeneous
21	Y	Isolated		21	Y	Amalgamated	
22	N		Inverse of expected	22	N		Homogeneous
23	Y	Amalgamated		23	Y	Amalgamated	
24	Y	Amalgamated		24	N		Homogeneous-linear
25	N		Inverse of expected	25	Y	Amalgamated-linear	
26	N		Inverse of expected	26	Y	Amalgamated-linear	
27	N		Inverse of expected	27	N		Inverse-linear
28	N		Homogeneous	28	N		Homogeneous-linear
29	Y	Amalgamated		29	N		Homogeneous-linear
30	N		Homogeneous	30	Y	Linear	
31	N		Inverse of expected	31	N		Inverse
32	N		Non conform	32	N		Inverse-linear
33	N		Homogeneous	33	N		Homogeneous-linear

Concerning permeabilities, only moderate- to high-permeability facies CK2 and CK3 were investigated. Ellipsoids display the same dominant N055 orientation. However, the CK2 and CK3 facies ellipsoids axis parametres are different. The anisotropy in CK2 is less important than in CK3 (Fig. 6). This variation in axis dimensions implies a differential behaviour of the associated geobodies. CK2 facies geobodies display mainly linear N055 orientations (Fig. 6). An alternative secondary N120–N140 direction is also apparent in this facies. CK3 facies geobodies display comparable behaviour to FF2

facies being mainly organised in groups of several geobodies that constitute a 1.5–2 km wide and 1 km long geobodies (Fig. 6).

4.4. Connectivity of simulated high permeability zones

Seven areas were selected to investigate the connectivity along and between fractured geobodies (sector 1 to sector 7): results obtained from the static connectivity algorithm (see Section 3.3) are synthesised in Fig. 7.

	Sp_Grignantes			Sp_Font-Reynaude		
	Fissures	Fractures	Azimuths	Fissures	Fractures	Azimuths
Sector 1	0.18181818	0.09090909	N021	0.4545455	0.333333333	N065
Sector 2	0.03030303	0.09090909	N029	0.2727273	0.303030303	N052
Sector 3	0.15151515	0.03030303	N076	0.3636364	0.242424242	N094
Sector 4	0.18181818	0.03030303	N064	0.3939394	0.303030303	N090
Sector 5	0.06060606	0.06060606	N022	0.2121212	0.303030303	N051
Sector 6	0.06060606	0.06060606	N015	0.1818182	0.363636364	N043
Sector 7	0.15151515	0.09090909	N000	0.3636364	0.424242424	N053
Average values	0.11688312	0.06493506		0.3203463	0.324675325	
Standard deviation	0.06411215	0.02726471		0.100286	0.057267344	

	Sp_Laurons			Sp_Grande-Bastide		
	Fissures	Fractures	Azimuths	Fissures	Fractures	Azimuths
Sector 1	0.54545455	0.57575758	N059	0.7272727	0.484848485	N115
Sector 2	0.36363636	0.39393939	N047	0.5151515	0.424242424	N057
Sector 3	0.42424242	0.39393939	N092	0.4848485	0.212121212	N125
Sector 4	0.48484849	0.54545455	N087	0.5454545	0.363636364	N127
Sector 5	0.3030303	0.36363636	N045	0.5757576	0.393939394	N061
Sector 6	0.3030303	0.45454546	N035	0.5757576	0.393939394	N041
Sector 7	0.45454546	0.60606061	N041	0.6666667	0.575757576	N175
Average values	0.41125541	0.47619048		0.5844156	0.406926407	
Standard deviation	0.09234082	0.09852647		0.0851982	0.111830284	
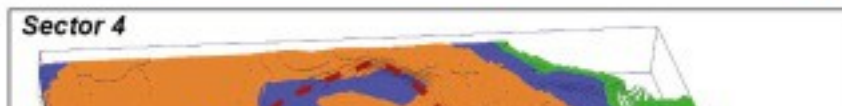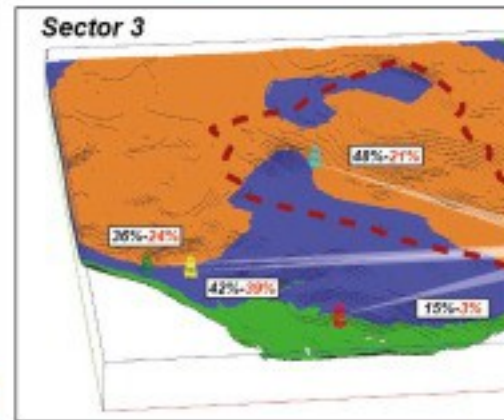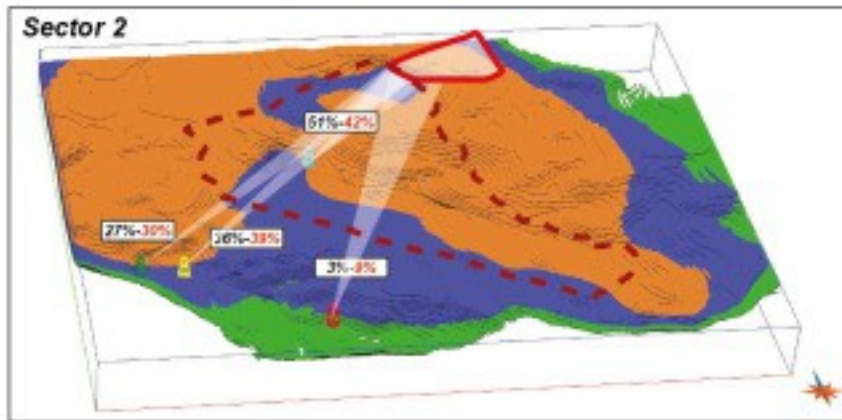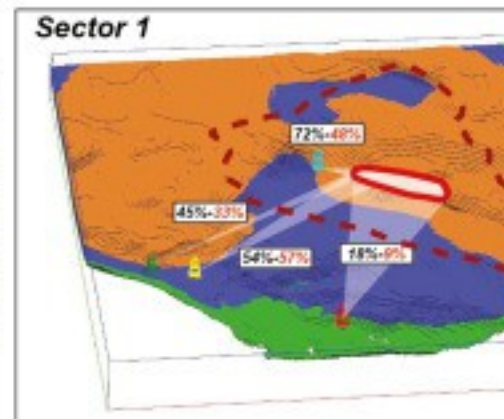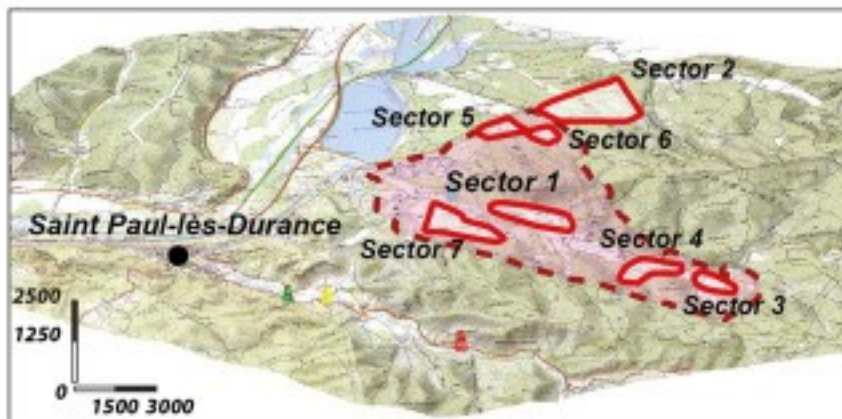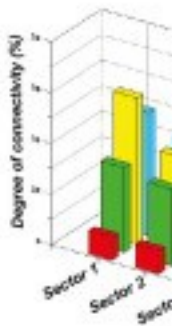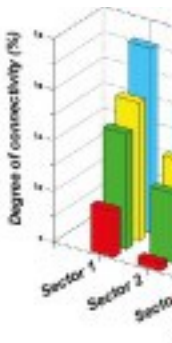
Fig. 7. Bar diagram and map of static connectivity probability inside and between geobodies containing major springs and seven sectors in the domain.

The probability of a connection between the different sectors and the Grignantes Spring is very low, ranging from 3% to 18%. This spring appears to be disconnected from these areas, even though sector 4 is oriented in the close direction of fractured geobodies.

The Font Reynaude Spring is connected to sectors 1 via CK2 facies (45%) and 7 via CK3 facies (42%). These sectors are closely oriented (azimuth N065 and N053) in the same axes as fractured geobodies (N055) this accounts for the high probabilities of connectivity displayed in this case.

Laurons Springs are mainly connected with sectors 1 (54%, via CK2), 7 (60%, via CK3), 4 (48%, via CK2 and 54%, via CK3) and 3 (42%, via CK2). Sectors 1 and 7 are closely oriented in the direction of fractured geobodies explaining the static connections within permeable geobodies through the western part of the Combe Fault system. Sectors 3 and 4 are not connected via the same direction (~N090). This direction does not correspond to the main [fracture orientation](#). This implies that the connectivity in that direction is controlled by another parameter (smaller scale fracture, sedimentary body). The Grande Bastide Spring is principally connected with sectors 1 (72%, via CK2 and 57%, via CK3), 7 (66% via CK2 and 48%, via CK3), 6 (57% via CK2), 5 (57% via CK2) and 2 (51% via CK2). Sector 1 is connected to the spring via a fault system parallel to the Cadarache Valley orientation (filled by Tertiary porous deposits). It is notable that sector 2, 5 and 6 are strongly connected with the spring. Low probabilities were obtained for connectivity between these sectors and springs located on the south of Cadarache Valley. This implies that a hydraulic barrier occurs between the northern and southern part of Cadarache Valley.

The connectivity with the different sectors can be summarised as follows:

–

     The connectivity with the Grignantes Spring is very low (6–11%).

     –

The connectivity with the Grande Bastide springs is higher via CK2 facies (58%) than via CK3 facies geobodies, suggesting a greater effectiveness of the CK2 facies geobody in the domain.

–

The connectivity with the Laurons Spring is slightly higher via a CK3 than via a CK2 geobody.

–

The connectivity with the Font Reynaude Spring is similar between CK2 and CK3 geobodies.

These results will be discussed in terms of their influence on the global water flow in the hydrogeological basin in Section 5.4.

5. Discussion

5.1. Benefit of the input of *a priori* data in stochastic model?

5.1.1. Fracture vertical proportion curve

Proposed by Cherubini et al. (2009) and by Yarus et al. (2012), the facies vertical proportion curve (VPC) can be a powerful tool to integrate geological heterogeneity in a 3D model. The aim of this cumulative histogram is to visualise the facies variability within a sedimentary succession or within selected stratigraphic units. This method was applied to the fracture facies FF1 to FF3. One of the objectives was to identify possible intra-stratigraphic variability of fracture proportion and to use it as *a priori* knowledge to force the model.
The obtained VPC emphasises the bias induced by the depth and the repartition of wells. This is because wells are dedicated to a hydrogeological network survey and are therefore mainly superficial. Moreover, the screened interval is highly variable. Consequently, the number of usable samples for the VPC is 182 in the Formation (3), 142 in Formation (2), and 37 in Formation (1). This bias prevented the use of VPC as a secondary input dataset for the model.

5.1.2. Relationship between Fracture density and faults location

Proposed by Caine et al. (1996), a fault zone is defined as the volume composed by a fault core and a damaged zone. The damaged zone is a key conduit or barrier for fluid flowconferring a marked local anisotropy to the permeability tensor. Yet, the thickness of these zones remains of prime importance in order to define fluid drains. For

instance, Matonti et al. (2012) conducted a petrophysical and structural characterisation of a fault zone in south-east France. They emphasised that the porous and permeable zone could be defined, on average, as a 20 m thick zone on both sides of the fault core. Similar petrophysical features were investigated here at the scale of the 3D model. Firstly, fracture orientation measured at the outcrop scale was compared to the main fault orientation. Fractures display two main orientations N040–N060 and N130–N140 comparable to fault orientations observed in the field and introduced in the 3D structural model. This observation matches the model of Micarelli et al. (2006), who studied highly porous carbonates from the Hyblean Plateau (Italy) and defined the damaged zone as an intense fault related fracture zone. Consequently, a second investigation was conducted here, focusing on the relationship between the distance to the fault and the proportion of fractured facies in wells. Due to the low amount of available data close to faults, the first region starts at 20 m from the fault plane. Then, regions are computed every 10 m from 20 to 100 m, every 20 m from 100 to 200 m, and every 200 above 200 m from fault. Error bars were calculated for each data point and range from 0% to 18% (Fig. 8). Data with error bars lower than 11% only (arbitrary cut-off avoiding most pronounced errors) are plotted and show 3 zones:

(i)

zone of intense fracturing with a fracture facies proportion higher than 88%;

(ii)
fractured zones far from faults with a proportion of non-fractured and fractured facies slightly varying around 40–60% respectively;

(iii)
unexpected proportion zones where the fractured to non-fractured facies ratio is the opposite of what is expected.
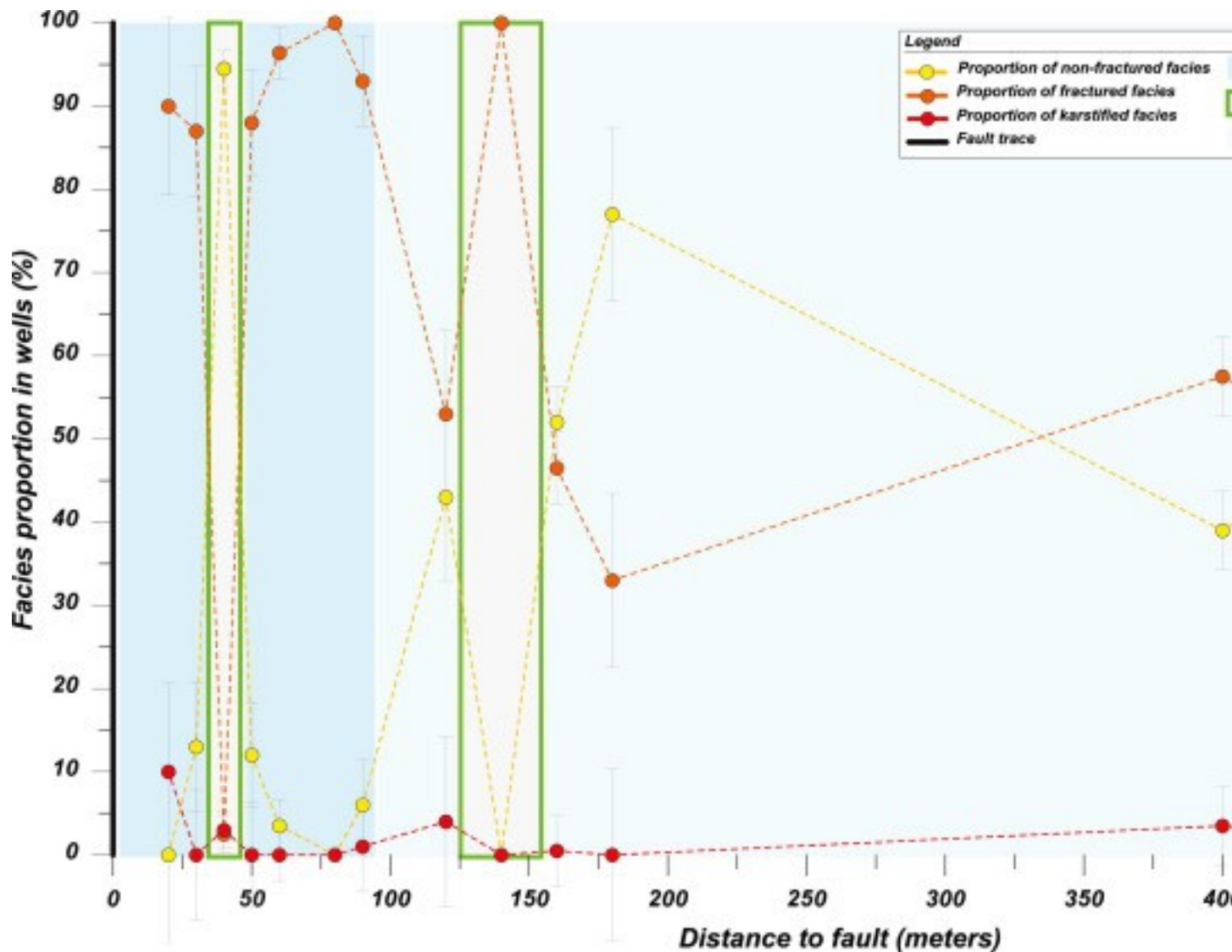
Fig. 8. Graph representing the facies proportion vs. the fault distance. Yellow dots are non-fractured facies, orange dots are fractured facies and red dots are karstified facies. Red zones are intense fracturation zones. Yellow zones represent the average proportion of fractured versus non-fractured facies calculated in all the boreholes. (For interpretation of the references to colour in this figure legend, the reader is referred to the web version of this article.)

The proximal 0–30 m zone is consistent with the previously defined fault zone. In this interval, the highly fractured facies are abundant. Nevertheless, between 30 and 40 m the proportion changes drastically with the proportion of non-fractured facies increasing to 94%. Between 40 and 90 m, the proportion of fractured facies resumes to a proportion comparable to the one observed close to the fault. Between 90 and 120 m

from the fault, the fracture facies to non-fractured facies ratio decreases again. The proportion of each facies reach values comparable to the mean proportion value calculated with the entire well dataset (42% non-fractured, 55% fractured). Between 120 and 130 m to the fault, another inversion occurs. The fractured facies reaches 100%. Finally, above 130 m, non-fractured and fractured facies again reach mean values observed at the whole dataset scale.

This investigation highlights the complexity of the relationship between faults and fractures, and the difficulty to constrain this relationship given the well data arrangement. Nevertheless, the 0–30 m from fault region is consistent with the definition of a fault damaged zone. Since it cannot be extended to 100 m (which is the size of the model elementary grid), damage around the main faults was not considered in the simulation processes.

5.2. Geological meaning of variographic analyses

Gringarten and Deutsch (1999) introduced variograms as a widely used tool to model the multi-scale heterogeneity in reservoirs. A major part (around 90%) of the geostatistical properties simulations of a reservoir are based on variographic analyses. The methodology generally adopted to interpret the variogram in order to compare to geological structures is to identify: (i) Small-scale correlations, mainly represented by the "nugget effect"; (ii) the intermediate-scale correlation corresponding to a geometric anisotropy; and (iii) the large-scale variability attributed to zonal anisotropy, hole-effect and trend behaviour (Gringarten and Deutsch, 2001).

In the present case study, no small-scale correlations have been identified. This indicates that the fracture facies and the permeability facies display intermediate to large scale anisotropy only. Field observations conducted on fractures are consistent with this approach. The small-scale heterogeneity described in previous studies (Bruna et al., 2013, Cartalade, 2002) was not taken into account because the upscaling process requiring interpolation of small-scale heterogeneity at the reservoir-scale was beyond the scope of this study. The reservoir behaviour is in this case was therefore considered as fracture flow driven only.

The intermediate-scale variability is obvious in the geometric anisotropy in FF1 and FF2 facies and in CK1 and CK3 facies (Appendices A and B). For all these facies, the maximum range is oriented in the N055 direction which matches the N040–N060 oriented faults. The maximum range of FF1 and FF2 is much higher than the range of CK1 and CK3. This is quite surprising because CK1 and CK3 represent permeability

values of matrix and fractured facies, respectively. This finding shows that the repartition of the permeability in fracture facies is heterogeneous.

Another interesting point is that moderate- and high-permeability facies (CK2-3) do not always match with fracture facies geobodies (FF2) (Fig. 6). This emphasises a paradox: the representation of FF1 and FF2 only reflects a part of the organisation of fractured geobodies; or the high permeability values (CK3) could be located in non-fractured areas. Indeed, high values of permeability could be attributed to porous intervals of Formation (3) ranging from 0 to more than 8%. The porosity values measured in several locations in Formation (3) are randomly distributed and could also correspond to isolated patches of high permeability. This configuration is in agreement with work from Ellis et al. (2012), demonstrating that long and open fractures can occur in damaged zones in a rock that is elsewhere nearly devoid of fractures.

The large-scale variability is represented by the hole-effect and the zonal anisotropy (Appendices A and B). In the case study, hole-effects are visible on the N180-125-110 azimuths only. The periodicity of the hole-effect is 50% higher in the N180 azimuth than in the two other directions. This is consistent with the observed periodic occurrence of N040-060 faults displaying a double period of 300 m and of 1000 m, indicating that the fault pattern should also affect the Northern part of the Cadarache Valley where the faults were not observed because of the Tertiary sedimentary covering.

The zonal anisotropy was observed in all the vertical variograms and a trend in some horizontal directions could explain a decreasing or an increasing of the intensity of a facies in the direction where the trend is defined (Appendices A and B). In both cases, these behaviours imply a continuity of a given facies in the considered direction. Zonal anisotropy or trend direction are generally associated to a perpendicular hole-effect (Guyonnet-Benaize et al., 2011), which occurs in FF2 and CK2 facies. Indeed, the FF2 facies display a slight trend in N077 direction and a zonal anisotropy in N180 direction. The CK2 facies display a zonal anisotropy in N055 direction and a hole-effect on N125 direction. Consequently, fractured geobodies and moderate permeability geobodies are mainly vertical and restricted to small-extended areas.

This type of analysis is uncommon because it uses SIS to represent fracture and permeability facies. Several authors proposed methods to simulate fractures as surfaces distributed in the model according to density and dimension distribution (Cherpeau et al., 2010, Bonneau et al., 2013). On the other hand, the SIS technique is a stochastic procedure commonly used for reproducing facies organisation (Guyonnet-Benaize et al., 2011, Felleti, 2004). In this paper, the SIS technique is used to reproduce the geometry and the organisation of fracture and permeability facies in the targeted

area. In that way, fractures are not considered as punctual objects but as volume of fracture facies. This appears to be particularly useful when diffuse fracturation takes place as well as fracturation linked to fault damaged zones.

5.3. Hydrogeological data representativity

Slug tests are widely used in hydrogeology because they are a low cost, quick tool to investigate the transmissivity and the storage capacity of aquifers. Interpretation of this kind of test has been extensively investigated by several authors (Papadopulos et al., 1973, Cooper et al., 1967, Black, 1985, Warner et al., 2006, Brauchler et al., 2010) in both homogeneous and fissured aquifers. Yet, an accurate characterisation of transmissivity in fractured media implies considering a wide range of parametres linked to the intrinsic fracture heterogeneity (complex combination of various sizes, apertures, filling materials, orientations, occurrence frequency). Such complexity is rarely considered in models of fractured aquifers. Some authors discussed this paradox and developed recommendations to best describe the aquifer heterogeneity. Shapiro and Hsieh (1998) compare transmissivity values obtained from slug tests realised on variable screened intervals ranging from 5 to 160 m in length. Transmissivity values obtained in these intervals vary over 5–6 orders of magnitude. The authors linked these variations to the presence of fractures. In order to decipher the impact of the model used to interpret the slug test in a fissured aquifer, the authors compare: (i) a mathematical solution considering the homogeneity of the aquifer and (ii) a Laplace Transform model taking into account fractures in the reservoir. It appears that transmissivity values obtained from both models always displayed less than one order of magnitude difference.

A Previous study (Bruna et al., 2013) highlights the strong variability in fracture type in the studied aquifer. According to Shapiro and Hsieh (1998), considering all these parametres generates an unpracticable complex model. Selection of most prominent fracture parametres is therefore required to represent the aquifer heterogeneity. Yet, the most transmissive fractures need to be prioritized, bearing in mind that the connectivity of the fracture network formed in part by smaller and less active faults will exert a strong control on solute contaminant transport especially in case of exchange between the fracture and the matrix (Parker et al., 2010, Parker et al., 2012) Then, the permeability heterogeneity related to the permeability of Lower Cretaceous hemipelagic limestone matrix ranging from 10^{-14} to 10^{-11} m s^{-1} (Cartalade, 2002) need to be addressed. The matrix heterogeneity was not introduced in the present models because of a paucity of data available to describe its repartition.

The question of the hydrogeological data representativity is also linked to the influence radius of a slug test. Due to the relatively low amount of water injected in the [borehole](#), the investigated zone is limited. [Guyonnet et al. (1993)](#) studied the volume of [porous media](#)investigated by a slug test in 3 theoretical cases. They note that the influence radius is easily identifiable in the case of homogeneous aquifers. They compared the return time to the static level in Cretaceous slug tests and the measured transmissivity of the aquifer. They were able to calculate influence radii ranging from millimetre to hectometre scales, highlighting that the increase of both permeability and influence radii is linked to geological structures such as matrix, fracture, fissures, faults and karsts. In our study, the influence radius previously described was used to define permeability ranges. In addition, fractures were taken into account by synthesising structural information gained from well logs and attributing specific well intervals to permeability ranges. This method reduced the bias induced by using averaged permeability values in the whole screened interval of the borehole.

5.4. Interest of the connectivity algorithm

The connectivity algorithm developed in this study is a useful tool to investigate the links between different permeable geobodies in a heterogeneous aquifer. It is of particular interest in the hydrogeological characterisation of highly discontinuous aquifers (fractured or karstic aquifers for example) where the number of data is in most cases not sufficient or difficult to integrate in a reservoir model (interference tests or tracer tests data).

Static connections between geobodies in a reservoir have already been used in several studies. [Lee et al. (2007)](#) use static connectivity in particularly high-K facies in California fluvial context. Results of this type of calculations may help identifying potential [groundwater flow](#) pathways and consequently preferential transport conduits in the reservoir. This assumption is conditioned by the use of dynamic data which were not developed in this study. Regarding other possible techniques of simulation on which connectivity should be applied [Falivene et al. (2006)](#) proposed a comparative study between outcrop evaluation of connected bodies and several simulation algorithms, including SIS simulation and concluded that the connectivity is often slightly overestimated in the case of SIS compared to other algorithms.
This overestimation is due to small-scale noise produced by this algorithm. We show in our study that this algorithm provides good results in static connectivity overview. The variability in volume of generated fractured and permeable geobodies illustrates that

their dispersion does not display a strong variability ([Fig. 9](#)). This assumption gives weight to connectivity interpretations.

Legend

- - - Mean curve of geobodies volume variability   —— Mean curve of fissured geobodies volume
—— Maximum curve of geobodies volume variability   —— Mean curve of fractured geobodies volume
—— Minimum curve of geobodies volume variability   —— Mean curve of fkarstified-faulted geobodies volume
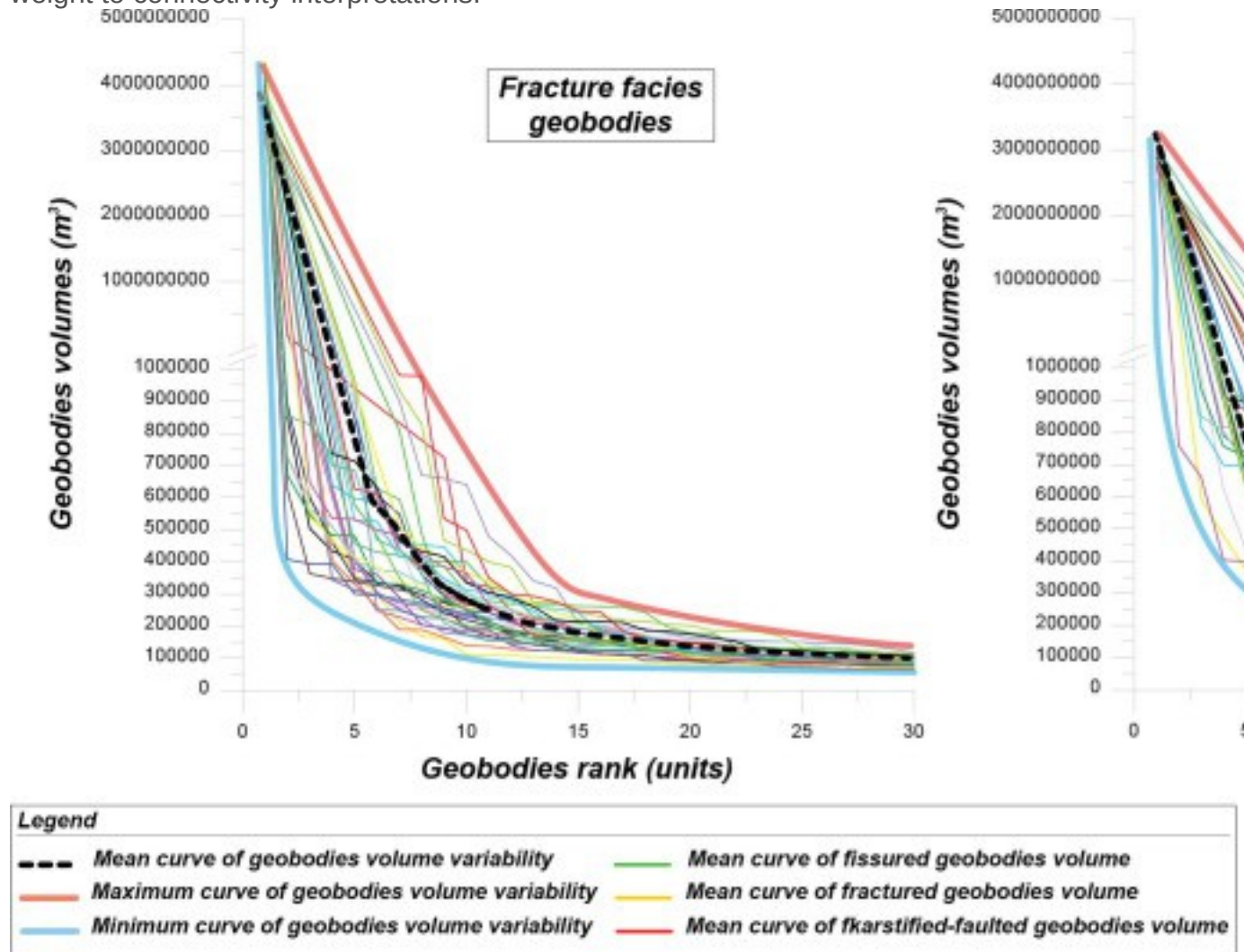
1. [Download high-res image (400KB)](#)
2. [Download full-size image](#)

Fig. 9. Geobodies sizes and ranks from the 33 simulations. Each coloured curve represents the data extracted from one simulation.

A map of the Cretaceous aquifer [water table](#) was produced, based on the monitoring of 68 [piezometers](#) connected to the Cretaceous aquifer, corresponding to April 2009 high water table ([Fig. 10](#)). Flow gradients display a first order direction from the SE towards the Durance River and a second order anomaly characterised by a complex high hydraulic gradient in the Mourre-Frais Valley towards the Durance (NW) and the Bete [ravine](#) (NNE). This high gradient can highlights (i) a low permeability zone parallel to the orientation of the valley that could correspond to the Tertiary deposits filling the up to 100 m thick paleo-valley incised in the Cretaceous formations and/or (ii) a high

permeability (fractured) drainage zone in the Cretaceous aquifer located on the left side of the valley (Fig. 10).
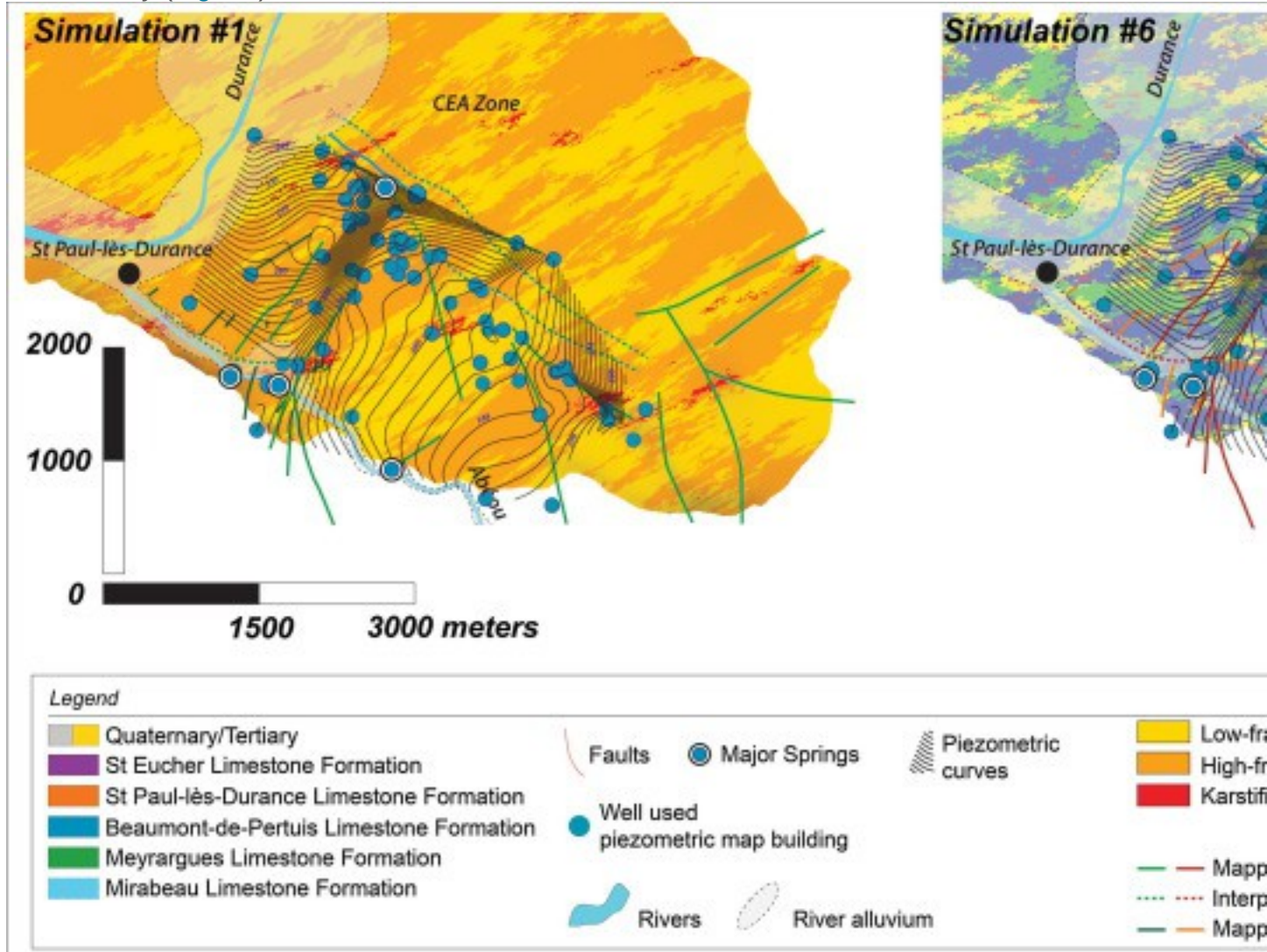
1. Download high-res image (1MB)
2. Download full-size image

Fig. 10. Geological map associated with piezometric levels measured in Lower Cretaceous aquifer in high water mark context (April 2009). Piezometric map is compared to fracture facies and permeability facies simulation in order to explain the tightening of isovalues of hydraulic head close to the Mourre-Frais zone.

The regional hydraulic flow does not follow the trend obtained from facies simulations. Then the uncertainties induced by the cluster distribution of the wells and by the shallow depth of investigation of the hydrogeological survey could play a role on these results. Nevertheless, it seems that the boundary conditions (topography in the SE and the Durance River in the NW of the domain) have a stronger influence on the hydraulic

gradient than the distribution of the reservoir properties. Interestingly, the high hydraulic gradient in the Mourre-Frais Valley matches a high fracture and fault density zone that was identified on 39% of the fracture facies simulations, and 41% of the permeability facies simulations, and where connected permeable geobodies are oriented parallel to the valley azimuth (Fig. 10).

6. Conclusions

Coupled integration in a three-dimensional geostatistical model of hydrogeological data (slug test method) and geological informations (sedimentary and fracture facies) from wells is an efficient way to characterise fissured aquifers. The 3D structural model first is way to integrate 1D, 2D and 3D data. Using the implicit method allows reducing artifacts close to geological unconformities, and gives the opportunity to quickly update the model.

This method results in a highly consistent stratigraphic grid even if modelling strategy is strongly influenced by the compromise between model resolution and computational performance that in the case of a highly fractured and faulted reservoir, may lead to the minimisation of fault offsets and smoothing of stratigraphic undulations.

An evaluation of the data consistency by comparison between field and well information provided before statistical modelling showed no unequivocal results that could be input into the model as secondary data. Consequently, simulations were only based on variographic anisotropy calculations and were realised for both fracture and permeability facies. We consider that this may be one of the most general cases since in much highly documented case there may be some potential correlations between facies and reservoir properties.

The key result of this modelling was to highlight the contrasted effects of fractures and faults on the reservoir permeability, permeable geobodies displaying a complex arrangement are much more influenced by faults than by fractured geobodies. The information provided by the model in terms of fracture anisotropy will be taken into account in hydrogeological modelling of the area.

The connectivity algorithm developed in this study allows computing the static connectivity between geobodies identified in the geostatistical modelling. The main flow orientation in this particular case does not follow the fracture and permeability facies because the piezometric gradient is primarily influenced by the topographic heights (SE) to the Durance River (NW). Such algorithms results still remain of great interest for pre-

dynamic modelling study currently used to characterise highly heterogeneous reservoirs.

Acknowledgements

Appendix A. Supplementary material

Low-fractured Facies

Vertical variogram

Azimuth 90

Azimuth 77

Azimuth 68

Azimuth 55

Azimuth 180

Azimuth 125

Azimuth 110

Azimuth 100

Fractured Facies

Vertical variogram

Azimuth 90

Azimuth 77

Azimuth 68

Azimuth 55

Azimuth 180

Azimuth 125

Azimuth 110

Azimuth 100

Karstified Facies

Vertical variogram

Azimuth 90

Azimuth 77

Azimuth 68

Azimuth 55
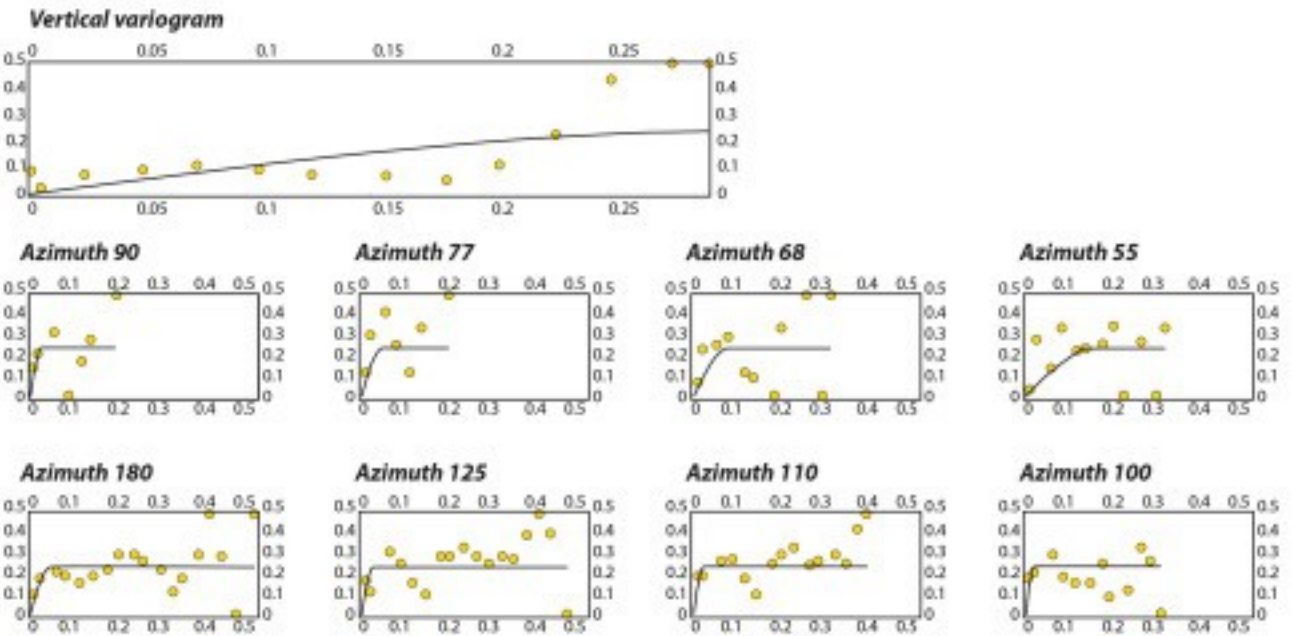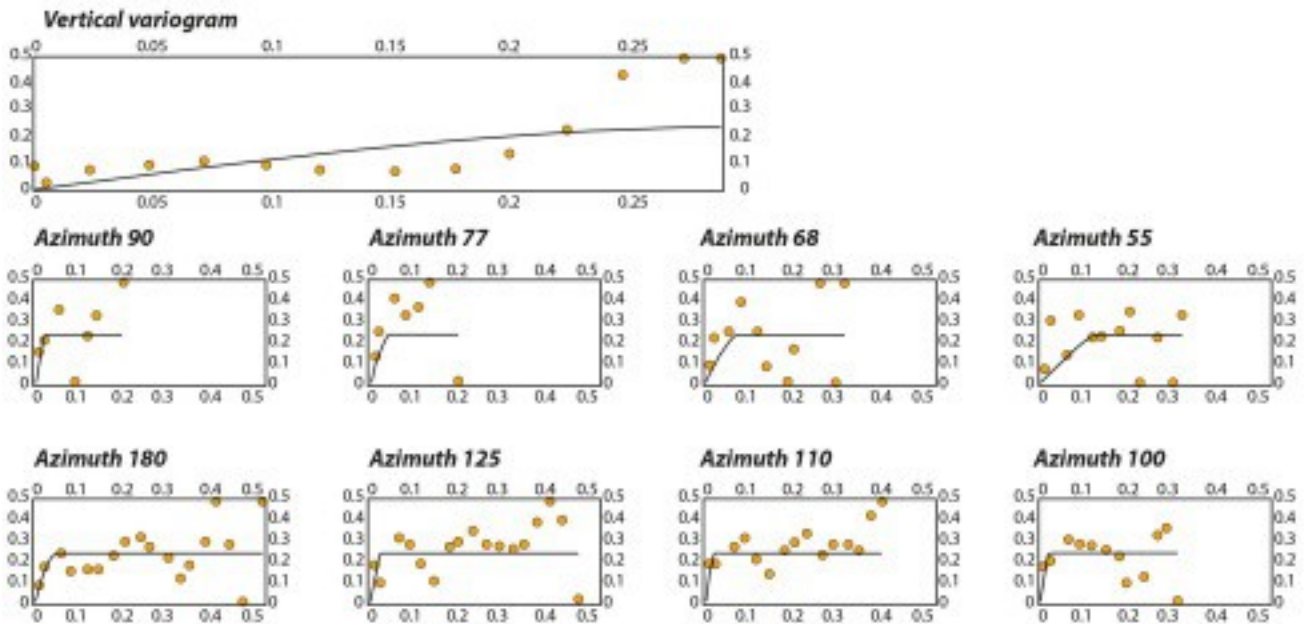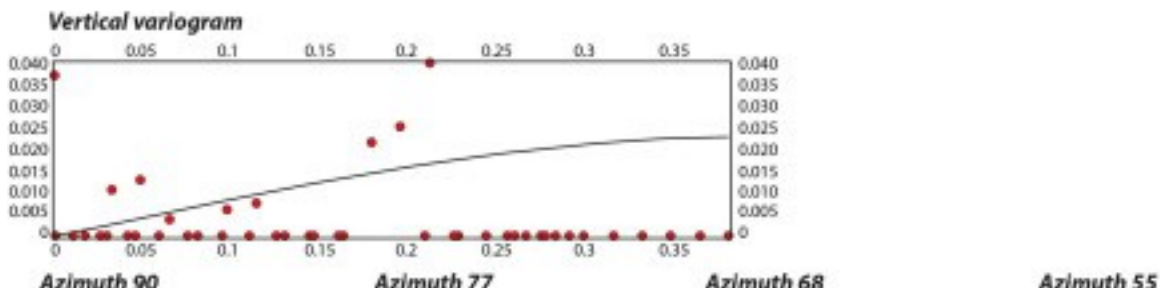
1. Download high-res image (791KB)
2. Download full-size image

Supplementary Figure 1.
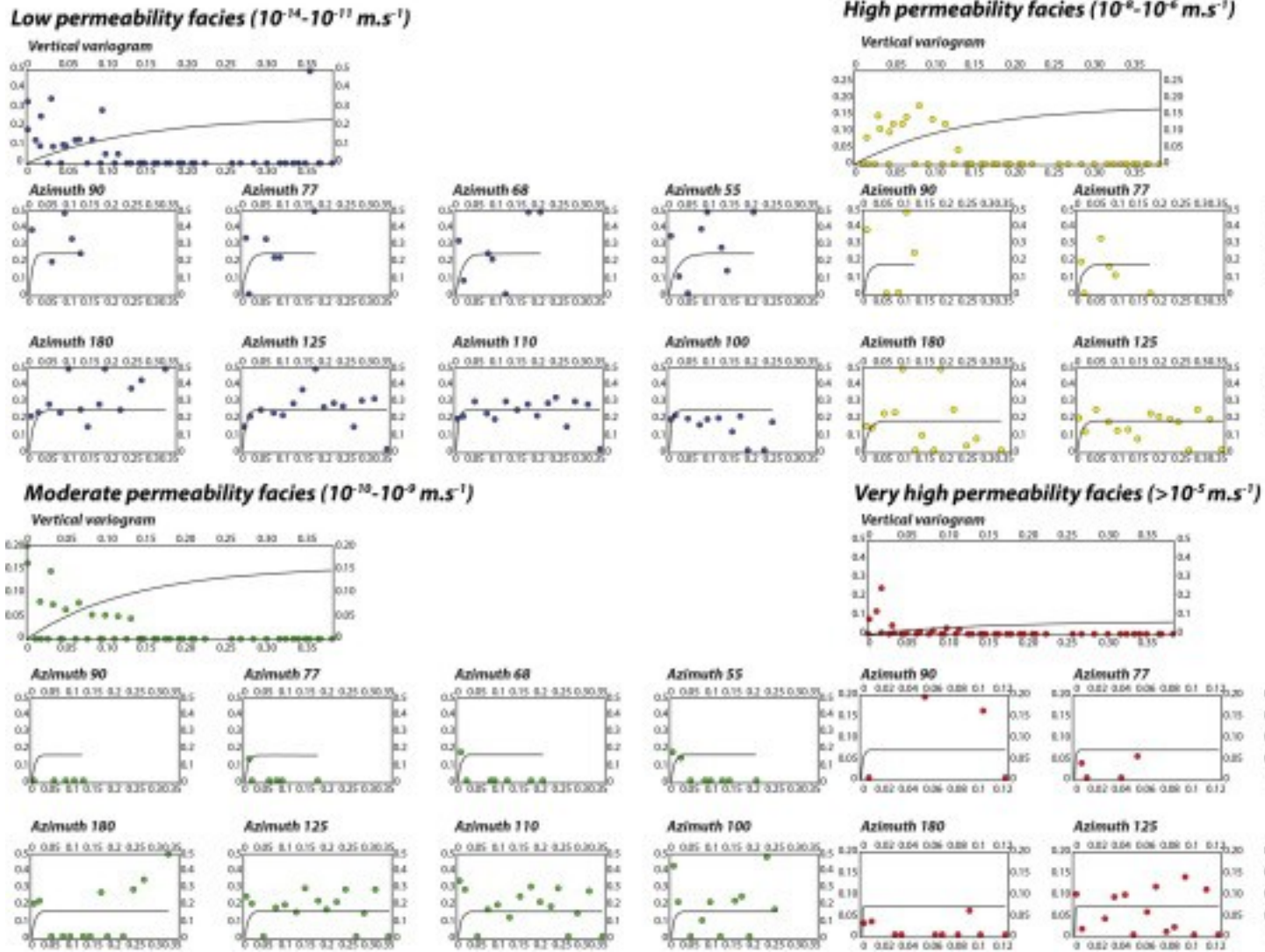
1. Download high-res image (767KB)
2. Download full-size image

Supplementary Figure 2.

References

Arlhac et al., 1970

Arlhac, P., Catzigras, F., Colomb, E., Gervais, J., Gouvernet, C, Guierard, S., et al. Carte géologique de Pertuis au 1/50 000e. Carte géologique détaillée de la France. In: Brgm (Ed.).

Armstrong, 1998

Armstrong, M., 1998. Basic Linear Geostatistics, Berlin, Germany.

[Bayer et al., 2011](#)

P. Bayer, P. Huggenberger, P. Renard, A. Comunian**Three-dimensional high resolution fluvio-glacial aquifer analog: Part 1: field study**

J. Hydrogeol., 405 (1–2) (2011), pp. 1-9

[ArticleDownload PDFView Record in Scopus](#)

[Berkowitz, 2002](#)

B. Berkowitz**Characterizing flow and transport in fractured geological media: a review**

Adv. Water Resour., 25 (2002), pp. 861-884

[ArticleDownload PDFView Record in Scopus](#)

[Biteman et al., 2004](#)

S. Biteman, D.W. Hyndman, M.S. Phanikumar, G.S. Weissmann**Integration of sedimentologic and hydrogeologic properties for improved transport simulations**

Aquifer Characterization, vol. 80, SEPM Special Publication (2004), pp. 4-13

[Black, 1985](#)

J.H. Black**The interpretation of slug tests in fissured rocks**

Q. J. Eng. Geol. Hydrogeol., 18 (1985), pp. 161-171

[CrossRefView Record in Scopus](#)

[Bonneau et al., 2013](#)

F. Bonneau, V. Henrion, G. Caumon, P. Renard, J. Sausse**A methodology for pseudo-genetic stochastic modeling of discrete fracture networks**

Comput. Geosci., 56 (2013), pp. 12-22

[ArticleDownload PDFView Record in Scopus](#)

[Brauchler et al., 2010](#)

R. Brauchler, R. Hu, T. Vogt, D. Al-Halbouni, T. Heinrichs, T. Ptak, *et al.***Cross-well slug interference tests: an effective characterization method for resolving aquifer heterogeneity**

J. Hydrol., 384 (2010), pp. 33-45, [10.1016/j.jhydrol.2010.01.004](#)

[ArticleDownload PDFView Record in Scopus](#)

[Bredehoeft and Papadopulos, 1980](#)

J.D. Bredehoeft, S.S. Papadopulos**A method for determining the hydraulic properties of tight formations**

Water Resour. Res., 16 (1980), pp. 233-238, [10.1029/WR016i001p00233](#)

[CrossRefView Record in Scopus](#)

[Bruna et al., 2013](#)

P.-O. Bruna, Y. Guglielmi, J. Lamarche, M. Floquet, F. Fournier, J.-P. Sizun, A. Gallois, L.Marié, C. Bertrand, F. Hollender**Porosity gain and loss in unconventional reservoirs: example of rock typing in Lower Cretaceous hemipelagic limestones, SE France (Provence)**

Mar. Pet. Geol., 48 (2013), pp. 186-205, [10.1016/j.marpetgeo.2013.08.008](#)

[ArticleDownload PDFView Record in Scopus](#)

[Caine et al., 1996](#)

J.S. Caine, J.P. Evans, C.B. Forster**Fault zone architecture and permeability structure**
Geology, 24 (1996), p. 4

Calcagno et al., 2008

P. Calcagno, J.P. Chilès, G. Courrioux, A. Guillen**Geological modelling from field data and geological knowledge: Part I. Modelling method coupling 3D potential-field interpolation and geological rules**
Phys. Earth Planet. Inter., 171 (2008), pp. 147-157, 10.1016/j.pepi.2008.06.013
ArticleDownload PDFView Record in Scopus

Carniero, 2009

J.F. Carniero**Numerical simulations on the influence of matrix diffusion to carbon sequestration in double porosity fissured aquifers**
Int. J. Greenhouse Gas Control, 3 (2009), pp. 431-443, 10.1016/j.ijggc.2009.02.006

Cartalade, 2002

A. Cartalade

Modélisation des écoulements dans les aquifères fracturés, developpement d'un modèle multi-continua (problèmes directs et inverse) et application au site du CEA/Cadarache, Université de Montpellier II, Montpellier (2002)

Cassan, 1978

Cassan, M., 1978. Les essais de perméabilité sur site dans la reconnaissance des sols, Tome I réalisation et interprétation. Eyrolles, Presse des ponts et chausses.

Caumon et al., 2009

G. Caumon, P. Collon-Drouaillet, C. Le Carlier de Veslud, S. Viseur, J. Sausse**Surface-based 3D modeling of geological structures**
Math. Geosci., 41 (2009), pp. 927-945, [10.1007/s11004-009-9244-2](10.1007/s11004-009-9244-2)
CrossRef[View Record in Scopus](View Record in Scopus)

Chapuis, 1998

R.P. Chapuis**Overdamped slug test in monitoring wells: review of interpretation methods with mathematical physical and numerical analysis of storativity influence**
Can. Geotech. J., 35 (1998), pp. 697-719
CrossRef[View Record in Scopus](View Record in Scopus)

Cherpeau et al.,

N. Cherpeau, G. Caumon, B. Lévy**Stochastic simulations of fault networks in 3D structural modeling**
C.R. Geosci., 342 (2010), pp. 687-694, 10.1016/j.crte.2010.04.008
Article[Download PDF](Download PDF)[View Record in Scopus](View Record in Scopus)

Cherubini et al.,

C. Cherubini, F. Musci, N. Pastore**Checking simulations of a geolithological model obtained by means of nested truncated bigaussian method**
Int. J. Math. Models Meth. Appl. Sci., 3 (2009), pp. 152-161
View Record in Scopus

Comunian et al.,

A. Comunian, P. Renard, J. Straubhaar, P. Bayer**Three-dimensional high resolution fluvio-glacial aquifer analog: Part 1: field study**
J. Hydrogeol., 405 (1–2) (2011), pp. 10-23
Article[Download PDF](Download PDF)[View Record in Scopus](View Record in Scopus)

Cooper et al., 19

H.H. Cooper Jr., J.D. Bredehoeft, I.S. Papadopulos**Response of a finite diameter well to an instantaneous change of water**
Water Resour. Res., 3 (1967), pp. 263-269
CrossRef[View Record in Scopus](View Record in Scopus)

Deutsch, 1998

C.V. Deutsch**Fortran programs for calculating connectivity of three-dimensional numerical models and for ranking multiple realizations**
Comput. Geosci., 24 (1998), pp. 69-76, [10.1016/S0098-3004(97)00085-X](10.1016/S0098-3004(97)00085-X)
Article[Download PDF](Download PDF)[View Record in Scopus](View Record in Scopus)

Ellis et al., 2012

M.A. Ellis, S.E. Laubach, P. Eichhubl, J.E. Olson, P. Hargrove**Fracture development and diagenesis of Torridon Group Applecross Formation, near An Teallach, NW Scotland: millennia of brittle deformation resilience?**
J. Geol. Soc. Lond., 169 (3) (2012), pp. 297-310, [10.1144/0016-76492011-086](10.1144/0016-76492011-086)
CrossRef[View Record in Scopus](View Record in Scopus)

Falivene et al., 2

O. Falivene, P. Arbués, A. Gardiner, G. Pickup, J.A. Muñoz, L. Cabrera**Best practice stochastic facies modeling from a channel-fill turbidite sandstone analog (the Quarry outcrop, Eocene Ainsa basin, northeast Spain)**
AAPG Bull., 90 (2006), pp. 1003-1029, [10.1306/02070605112](10.1306/02070605112)
CrossRef[View Record in Scopus](View Record in Scopus)

Felleti, 2004

F. Felleti**Statistical modelling and validation of correlation in turbidites: an example from the Tertiary Piedmont Basin (Castagnola Fm., Northern Italy)**
Mar. Pet. Geol., 21 (2004), pp. 23-39

Gilli et al., 2008

E. Gilli, C. Mangan, J. Mudry**Hydrogéologie: objets, méthodes, applications**
(second ed.), Dunod, Paris, France (2008)

Goovaerts, 1997

Goovaerts, P., 1997. Geostatistics for Natural Resources Evaluation, New-York.

Gréselle and Pitt

B. Gréselle, B. Pittet**Sea-level reconstructions from the Peri-Vocontian Zone (South-east France) point to Valanginian glacio-eustasy**
Sedimentology, 57 (2010), pp. 1640-1685
CrossRef[View Record in Scopus](View Record in Scopus)

Gringarten and D

Gringarten, E., Deutsch, C.V., 1999. Methodology for variogram interpretation and modeling for improved reservoir characterization. In: SoP Engineers (Eds.), Society of Petroleum Engineers Annual Technical Conference and Exhibition Houston, Texas, 1999, pp. 1–13.

Gringarten and D

E. Gringarten, C.V. Deutsch**Teacher's aide. Variogram interpretation and modeling**
Math. Geol., 33 (2001), pp. 507-533, [10.1023/A:1011093014141](10.1023/A:1011093014141)
CrossRef[View Record in Scopus](View Record in Scopus)

Guerriero et al.,

V. Guerriero, S. Mazzoli, A. Iannace, S. Vitale, A. Carravetta, C. Strauss**A permeability model for naturally fractured carbonate reservoirs**
Mar. Pet. Geol., 40 (2013), pp. 115-134
Article[Download PDF](Download PDF)[View Record in Scopus](View Record in Scopus)

Guo and Deutsch

H. Guo, C.V. Deutsch**Fluvial channel size determination with indicator variograms**
Petrol. Geosci., 16 (2010), pp. 161-169
CrossRefView Record in Scopus

Guyonnet et al.,

D. Guyonnet, S. Mishra, J. McCord**Evaluating the volume of porous medium investigated by slug tests**
Ground Water, 31 (1993), pp. 627-633
CrossRefView Record in Scopus

Guyonnet-Benaiz

C. Guyonnet-Benaize**Modélisation 3D multi-échelle des structures géologiques de la région de la Faille de la Moyenne Durance (SE, France)**
Université de Provence, Marseille (2011)

Hooker et al., 20

J.N. Hooker, S.E. Laubach, R. Marrett**Fracture-aperture size-frequency, spatial distribution, and growth processes in strata-bounded and non-strata-bounded fractures, Cambrian Mesón Group, NW Argentina**
J. Struct. Geol., 54 (2013), pp. 54-71, 10.1016/j.jsg.2013.06.011
ArticleDownload PDFView Record in Scopus

Knudby and Car

C. Knudby, J. Carrera**On the relationship between indicators of geostatistical, flow and transport connectivity**
Adv. Water Resour., 28 (2005), pp. 405-421, 10.1016/j.advwatres.2004.09.001
ArticleDownload PDFView Record in Scopus

Lamarche et al.,

J. Lamarche, A.P.C. Lavenu, B.D.M. Gauthier, Y. Guglielmi, O. Jayet**Relationships between fracture patterns, geodynamics and mechanical stratigraphy in Carbonates (South-East Basin, France)**
Tectonophysics (2012), 10.1016/j.tecto.2012.06.042

Laubach et al., 2

S.E. Laubach, J.E. Olson, M.R. Gross**Mechanical and fracture stratigraphy**
AAPG Bull., 93 (2009), pp. 1413-1426
CrossRefView Record in Scopus

Lee et al., 2007

S.-Y. Lee, F.C. Carle, G.E. Fogg**Geologic heterogeneity and a comparison of two geostatistical models: sequential Gaussian and transition probability-based geostatistical simulation**
Adv. Water Resour., 30 (2007), pp. 1914-1932
ArticleDownload PDFView Record in Scopus

Loucks et al., 20

R.G. Loucks, R.M. Reed, S.C. Ruppel, U. Hammes**Spectrum of pore types and networks in mudrocks and a descriptive classification for matrix-related mudrock pores**

AAPG Bull., 96 (2012), pp. 1071-1098

CrossRefView Record in Scopus

Masse and Mass

J.-P. Masse, M. Masse**Notice du crétacé inférieur de la Basse-Durance**

Université de Provence, Marseille (2009)

pp. 19

Matonti et al., 20

C. Matonti, Y. Guglielmi, J. Lamarche, L. Marié**Structural and petrophysical characterization of mixed drain/barrier fault zones in carbonates: example from the Castellas Fault (SE France)**

J. Struct. Geol. (2012)

Mejìas et al., 200

M. Mejìas, P. Renard, D. Glenz**Hydraulic testing of low-permeability formations. A case study in the granite of Cadalso de los Vidrios, Spain**

Eng. Geol., 107 (2009), pp. 88-97

doi: 10.1016

ArticleDownload PDFView Record in Scopus

Mennessier et al

Mennessier, G., Modret, D., Goguel, J., 1966. Carte géologique de Tavernes au 1/50 000e. Cartes géologiques détaillées de la France. In: Brgm (Ed.).

Micarelli et al., 2

L. Micarelli, A. Benedicto, C.A.J. Wibberley**Structural evolution and permeability of normal fault zones in highly porous carbonate rocks**

J. Struct. Geol., 28 (2006), pp. 1214-1227, 10.1016/j.jsg.2006.03.036

ArticleDownload PDFView Record in Scopus

Motyka et al., 19

J. Motyka, A. Pulido-Bosch, S. Borczak, J. Gisbert**Matrix hydrogeological properties of Devonian carbonate rocks of Olkusz (Southern Poland)**

J. Hydrol., 211 (1998), pp. 140-150

ArticleDownload PDFView Record in Scopus

Nelson, 2009

P.H. Nelson**Pore-throat sizes in sandstones, tight sandstones, and shales**

AAPGs Bull., 93 (2009), pp. 329-340, 10.1306/10240808059

CrossRefView Record in Scopus

Papadopulos et al., 1973

I.S. Papadopulos, J.D. Bredehoeft, H.H. Cooper**On the analysis of slug test data**

Water Resour. Res., 9 (1973), pp. 1087-1089

CrossRefView Record in Scopus

Parker et al., 2010

B.L. Parker, S.W. Chapman, J.A. Cherry**Plume persistence in fractured sedimentary rock after source zone removal**

Ground Water, 48 (6) (2010), pp. 799-808

View Record in Scopus

Parker et al., 2012

B.L. Parker, J.A. Cherry, S.W. Chapman**Discrete fracture network approach for studying contamination in fractured rock**

AQUA Mundi, 3 (2) (2012), pp. 101-116

View Record in Scopus

Pöppelreiter et al., 2008

M.C. Pöppelreiter, M.A. Balzarini, B. Hansen, R. Nelson**Realizing complex carbonate facies, diagenetic and fracture properties with standard reservoir modelling software**

The Future of Geological Modelling in Hydrocarbon Development, vol. 309, The Geological Society, London, Special Publications (2008), pp. 39-49, 10.1144/SP309.3

CrossRefView Record in Scopus

Renard, 2003

P. Renard**Hytool: a Hydrogeological Toolbox**

University of Neuchâtel, Switzerland (2003)

Renard, 2007

P. Renard**Stochastic hydrogeology; what professionals really needs?**

Ground Water, 45 (2007), pp. 531-541

CrossRefView Record in Scopus

Renard and Allard, 2013

P. Renard, D. Allard**Connectivity metrics for subsurface flow and transport**

Adv. Water Resour., 51 (2013), pp. 168-196

ArticleDownload PDFView Record in Scopus

Rzonca, 2008

B. Rzonca**Carbonate aquifers with hydraulically non-active matrix: a case study from Poland**

J. Hydrol., 355 (2008), pp. 202-213

ArticleDownload PDFView Record in Scopus

Shapiro and Hsieh, 1998

A.M. Shapiro, P.A. Hsieh**How good are estimates of transmissivity from slug tests in fractured rocks?**

Ground Water, 36 (1998), pp. 37-48

CrossRefView Record in Scopus

Spottke et al., 2005

I. Spottke, E. Zechner, P. Huggenberger**The southeastern border of the Upper Rhine Graben: a 3D geological model and its importance for tectonics and groundwater flow**

Int. J. Earth Sci., 94 (4) (2005), pp. 580-593

CrossRefView Record in Scopus

Stampfli and Borel, 2002

G.M. Stampfli, G.D. Borel**A plate tectonic model for the Paleozoic and Mesozoic constrained by dynamic plate boundaries and restored synthetic oceanic isochrons**

Earth Planet. Sci. Lett., 196 (2002), pp. 17-33, 10.1016/S0012-821X(01)00588-X

ArticleDownload PDFView Record in Scopus

Warner et al., 2006

J.W. Warner, C. Tamayo-Lara, E. Khazaei, F. Manghi**Stochastic management modeling of a pump and treat system at the Rocky Mountain Arsenal near Denver, Colorado**

J. Hydrol., 328 (3) (2006), pp. 523-537

ArticleDownload PDFView Record in Scopus

Wu et al., 2004

Y.-S. Wu, H.H. Liu, G.S. Bodvarsson**A triple-continuum approach for modeling flow and transport processes in fractured rock**

J. Contam. Hydrol., 73 (2004), pp. 145-179, 10.1016/j.jconhyd.2004.01.002

ArticleDownload PDFView Record in Scopus

Yang and Gates, 1997

Y.J. Yang, T.M. Gates**Wellbore skin effect in slug-test data analysis for low-permeability geologic materials**

Ground Water, 35 (1997), pp. 931-937

CrossRef

Yarus et al., 2012

Yarus, J.M., Chambers, R.L., Maucec, M., Shi, G., 2012. Facies Simulation in Practice. Lithotype proportion mapping and Plurigaussian Simulation, a powerful combination. In: Ninth International Geostatistics Congress, Oslo, Norway, 2012.

Zou, 2013

C. Zou**Unconventional Petroleum Geology**

(first ed.), Elsevier Inc., China (2013)